Chapter 6

CHAPTER 6

GUM - BASED ON SOLID-STATE BIOPOLYMER ELECTROLYTES AND ITS APPLICATION TO ELECTROCHEMICAL STORAGE DEVICES

Renewable energy technologies are increasing in demand for future energy production, storage, and consumption. Naturally available biomaterials are growing in leaps and bounds as a source of bio-electrolyte for energy storage devices [1,2]. Solid-state biopolymer electrolytes have been developed to overcome the loopholes in liquid electrolytes, their fabrication, and production economy [3]. Thus, numerous bio-based solid polymer electrolytes and gel electrolytes have been explored and studied [4,5]. Gum from plant parts has a wide variety of applications in food packaging, drug delivery, biomedical fields, and much more [6–10]. Many interesting and bio-derived materials such as banana peel, tea leaves, bamboo powder, and coffee beans have been used as a source of activated carbon for supercapacitors, EDLC, and in battery applications [11–14].

In the present research, *Salmalia Malabarica* Gum (SG) has been chosen for the preparation of the bio-membrane by blending with polyvinyl alcohol (PVA) as in our previous work [15]. The first ever report using SG has been developed by solution casting technique with 1g SG + 0.8g PVA (SGBP) and optimized with impedance analysis by their highest ionic conductivity values as in Table 3.3. The ionic conductivity of the optimized membrane SGBP was found to be 3.11×10^{-5} S cm^{-1}

6.1 Investigation of SG as solid bio-electrolyte for ion-conducting Battery

To investigate the electrochemical properties of the *Salmalia Malabarica* Gum, obtained from the bark of the tree, this study has been performed. The SGBP electrolyte has been prepared by first blending SG with PVA and then by doping charge carriers $MgCl_2$, LiCl, and NH_4HCO_2 integrated into the bio-membrane composition. This prepared bio-electrolyte has been then characterized and fabricated for the ion-conducting battery.

6.1.1 *Preparation of the SGBP bio-membrane and its dopped bio-electrolyte:*

The bio-membrane has been prepared, using SG and PVA as discussed in Chapter 3. The bio-membrane of composition 1g SG + 0.8g PVA (SGBP) has been optimized with the highest ionic conductivity and selected for the bio-electrolyte preparation with magnesium chloride,

lithium chloride and ammonium formate as the dopants. The incorporation of the SMBP with the dopants in varying weight percentage ratios as 0.3wt% to 0.8wt% has been carried by uniform blending in a magnetic stirrer, ensuring the complete mixing of the ionic dopant into the bio-membrane composition 1g SG + 0.8g PVA for about 24hrs. Further, the blend solution has been cast into the polypropylene petri dishes and then evaporated in a vacuum, then the respective bio-electrolytes, SGMC (Figure 6.1), SGLC (Figure 6.2), and SGAF (Figure 6.3) membranes are stored in a desiccator for further analysis and characterization.

Figure 6.1: Biopolymer electrolyte membrane - SGMC

Figure 6.2: Biopolymer electrolyte membrane - SGLC

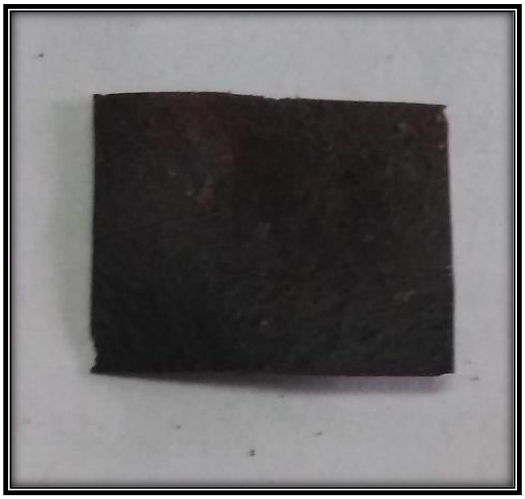

Figure 6.3: Biopolymer electrolyte membrane - SGAF

6.1.2 *X-ray Diffraction (XRD) Analysis*

6.1.2.1 *XRD for magnesium chloride doped SG bio-electrolyte- SGMC 0.7*

The diffraction pattern for the *Salmalia Malabarica* Gum (SG) and the biopolymer membrane SGBP are illustrated in Figures 6.4 and 6.5. Figure 6.6 represents the XRD pattern for magnesium chloride-doped bio-electrolytes SGMC 0.5, SGMC 0.6, SGMC 0.7, and SGMC 0.8. The X-ray diffraction pattern for the SG in Figure 6.4 shows semicrystalline peaks at $2\theta = 17.9°$, 26.6°, 44.4° and the blend SG with PVA in Figure 6.5 for the membrane SGBP shows peaks at 18.6°, 44.4°. The peaks found in SG have merged and broadened for SGBP due to the uniform blending of SG with PVA.

The peak observed at 19.3° corresponds to the PVA used to blend with SG for the preparation of the membrane SGBP [16]. The diffraction pattern in Figure 6.6 shows a broad hump with the incorporation of magnesium chloride into the biopolymer SGBP composition. The characteristic peak for the PVA and SG found in Figures 6.4 and 6.5 has broadened after the addition of ionic dopant in the bio-electrolyte membranes as observed in Figure 6.6. The broadness of the peak increases with an increase in the concentration of magnesium chloride to SG which affirms that the addition of magnesium salt remarkably enhances the amorphous nature of the bio-electrolyte membranes [17]. The increase in amorphous nature with the increase in salt concentration and their relationship with the relative intensity of the peak and degree of crystallinity follows Hodge et al evaluation [18]. It has to be noted that the peaks corresponding

to magnesium chloride were not observed for SGMC 0.5, SGMC 0.6, and SGMC 0.7. This ensures the complete dissolution of the dopant in the SGBP host composition.

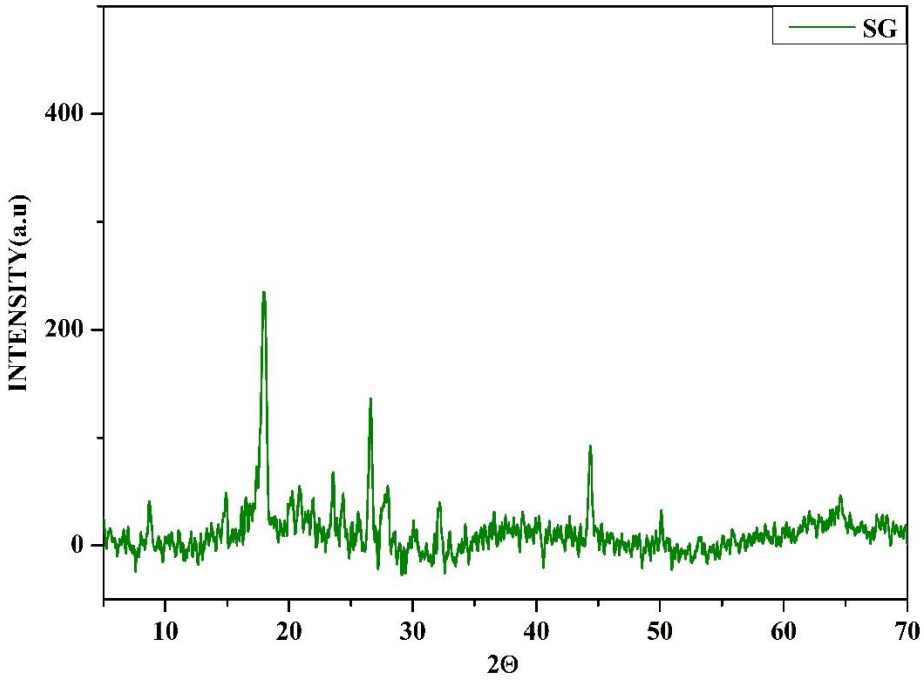

Figure 6.4: XRD pattern of SG

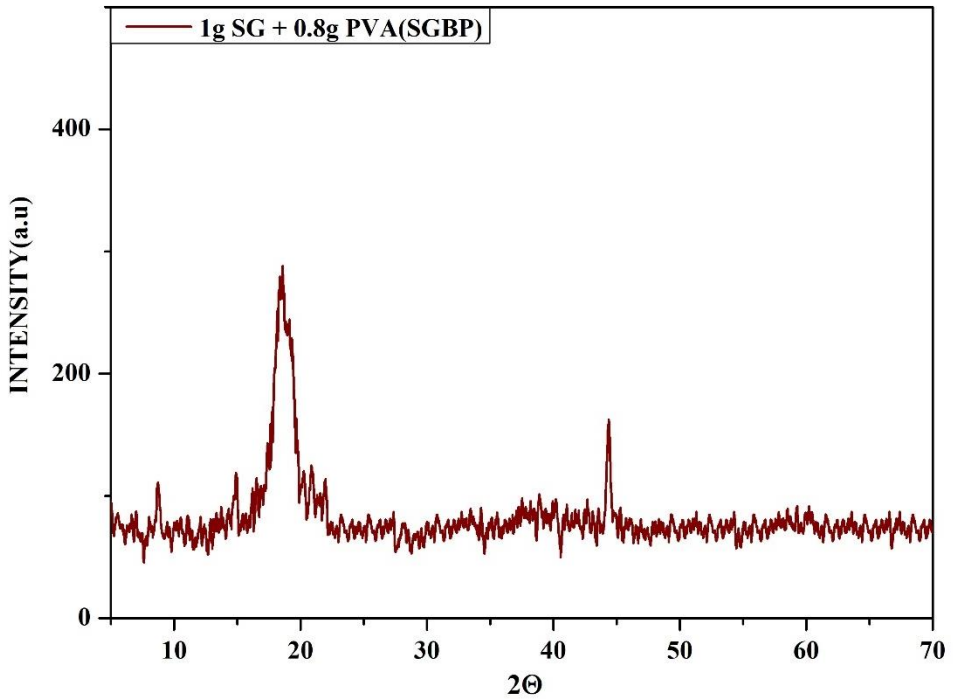

Figure 6.5: XRD pattern of SGBP (1g SG + 0.8g PVA)

The broadness of the peak is maximum for SGMC 0.6 as noticed in Figure 6.6 when compared to the other samples which are also evident from their degree of crystallinity values listed in Table 6.1. This amorphous nature of the membrane SGMC 0.6 aids in ionic mobility for the carrier ions, thereby enhancing the ionic conductivity of the membrane owing to the reduction in the energy barrier for the fragmental motion of the host matrix SGBP [19,20]. With further increase in the dopant concentration to 0.8wt% $MgCl_2$ into the host SGBP composition, shows peaks at 28.3° and 31.6° for the bio-electrolyte SGMC 0.8 which corresponds to $MgCl_2$. The introduction of new peaks for SGMC 0.8 membrane which accounts for the ionic dopant may be due to the recrystallization of the added salt in the host matrix SGBP [15]. There is a decline in the amorphous nature which is also obvious from the degree of crystallinity values in Table 6.1.

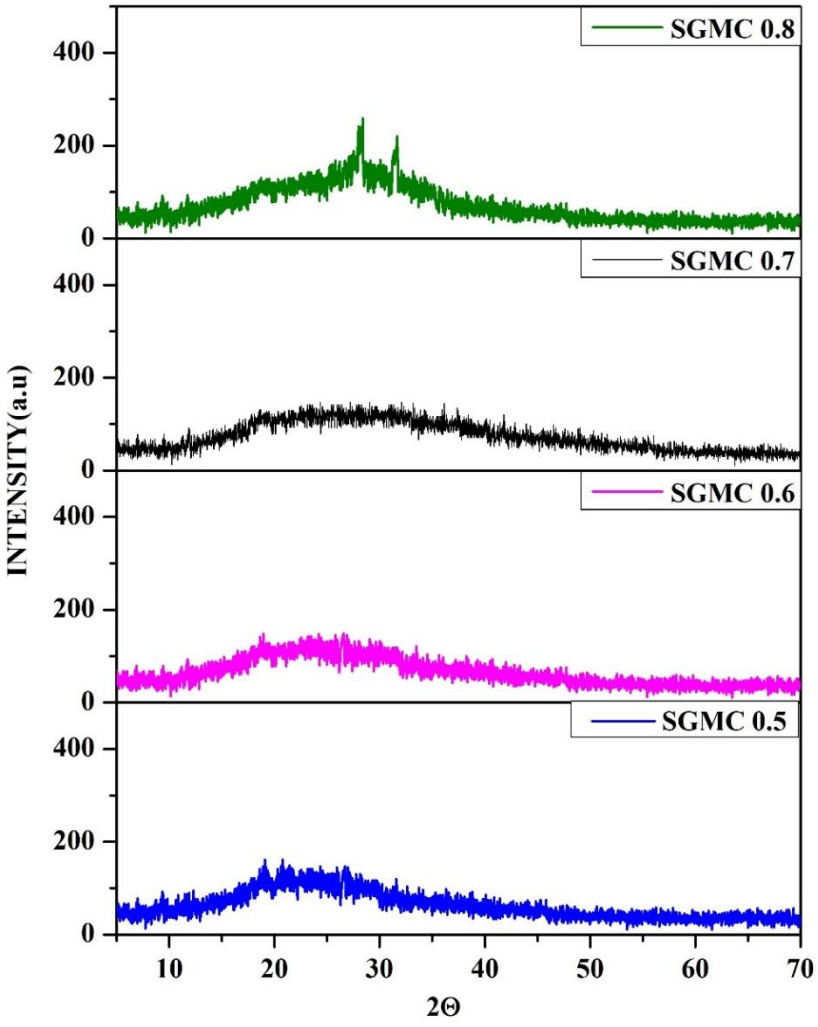

Figure 6.6: XRD pattern of SGMC 0.5, SGMC 0.6, SGMC 0.7, and SGMC 0.8

Table 6.1: Percentage of crystallinity for SGBP and SGBP with different concentrations of $MgCl_2$, LiCl and NH_4HCO_2

Composition	Percentage of Crystallinity
SGBP (1g SG + 0.8g PVA)	37.90
Magnesium chloride – doped SGBP bio-electrolytes	
SGBP + 0.5wt% $MgCl_2$ (SGMC 0.5)	21.05
SGBP + 0.6wt% $MgCl_2$ (SGMC 0.6)	18.34
SGBP + 0.7wt% $MgCl_2$ (SGMC 0.7)	**15.89**
SGBP + 0.8wt% $MgCl_2$ (SGMC 0.8)	19.27
Lithium chloride – doped SGBP bio-electrolytes	
SGBP + 0.3wt% LiCl (SGLC 0.3)	33.37
SGBP + 0.4wt% LiCl (SGLC 0.4)	25.89
SGBP + 0.5wt% LiCl (SGLC 0.5)	**14.55**
SGBP + 0.6wt% LiCl (SGLC 0.6)	22.36
Ammonium formate – doped SGBP bio-electrolytes	
SGBP + 0.5wt% NH_4HCO_2 (SGAF 0.5)	31.69
SGBP + 0.6wt% NH_4HCO_2 (SGAF 0.6)	28.40
SGBP + 0.7wt% NH_4HCO_2 (SGAF 0.7)	**18.21**
SGBP + 0.8wt% NH_4HCO_2 (SGAF 0.8)	27.10

6.1.2.2 *XRD for lithium chloride doped SG bio-electrolyte- SGLC 0.5*

The XRD pattern for the lithium chloride-doped bio-electrolytes SGLC 0.3, SGLC 0.4, SGLC 0.5, and SGLC 0.6 are depicted in Figure 6.7. With the addition of lithium chloride salt from 0.3wt% to 0.7wt% (SGLC 0.3 to SGLC 0.6) to the blend, SGBP composition has broadened the peak around 26.6° with a decrease in relative intensity. The peak observed at 17.9° in the XRD of SG has also been observed in SGLC 0.3 and with less intensity in SGLC 0.4 bio-electrolyte membranes. The decrease in peak intensity and broadening of the peaks with the addition of lithium chloride indicates the amorphous nature of the membranes as explained by Hodge et.al [18]. Thus, with the increase in lithium chloride concentration, there is also a decline in the degree of crystallinity in Table 6.1 as explained before for magnesium chloride-doped membranes.

This increase in amorphous nature with the increase in ionic dopant leads to high ionic conductivity [21] due to the distortion in the backbone of the host matrix SGBP [22,23] which facilitates the ease of ionic mobility through the bio-electrolyte membrane in the amorphous phase [24]. Among all the bio-electrolytes synthesized, SGLC 0.5 displays high amorphous nature which is also supported by the degree of crystallinity in Table 6.1. The absence of the peak concerning lithium chloride is also an indication of the complete disintegration of the salt in the host matrix SGBP [25].

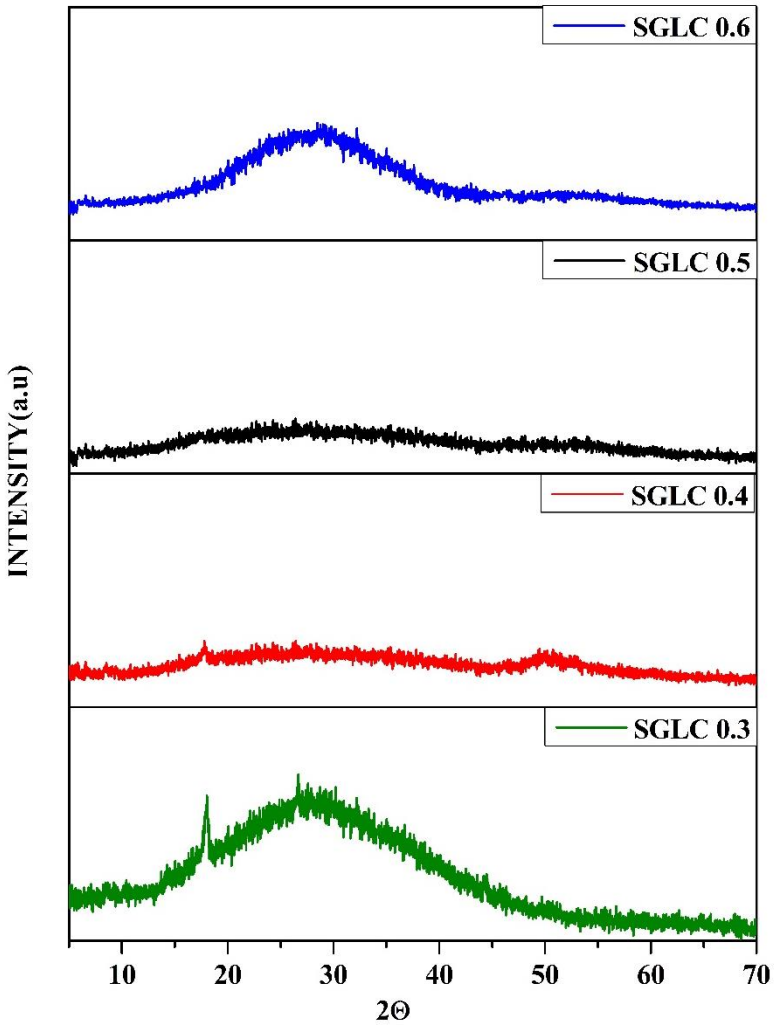

Figure 6.7: XRD pattern of SGLC 0.3, SGLC 0.4, SGLC 0.5, and SGLC 0.6

Hence the sample SGLC 0.5 has been expected to produce maximum ionic conductivity. Typically, as explained the amorphous nature of the bio-electrolyte increases with an increase in concentration, but after the tolerance limit of the SGBP host to accommodate the excess salt has reached there is an increase in the degree of crystallinity with an increase in relative intensity of the peak SGMC 0.6 bio-electrolyte film [26].

6.1.2.3 *XRD for ammonium formate doped SG bio-electrolyte- SGAF 0.7*

The amorphous peaks of the ammonium formate incorporated bio-electrolytes SGAF 0.5, SGAF 0.6, SGAF 0.7, and SGAF 0.8 are demonstrated in Figure 6.8.

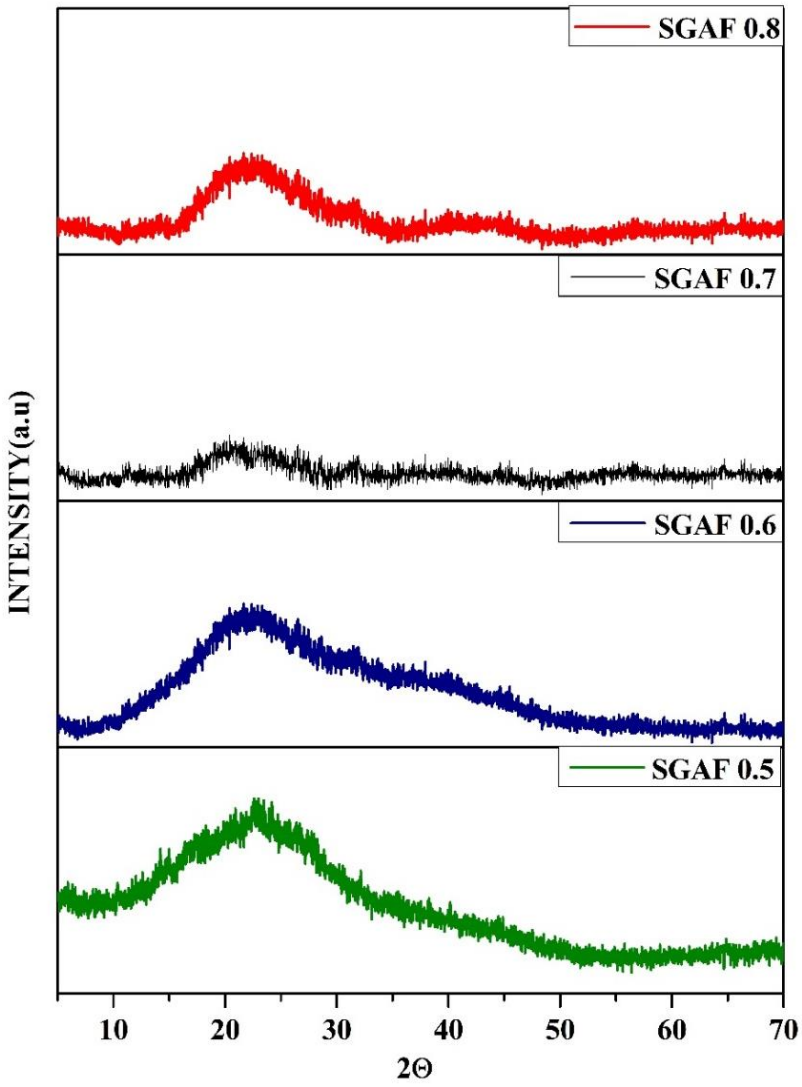

Figure 6.8: XRD pattern of SGAF 0.5, SGAF 0.6, SGAF 0.7, and SGAF 0.8

Upon integration of the ionic dopant, ammonium formate to the host matrix SGBP, the peak observed at 22.5° has broadened for all the bio-electrolytes. Similar to the above results, the enhancement of its amorphous nature increases with an increase in the concentration of the ionic dopant due to the complex formation of the salt with the host matrix and is obvious from the degree of crystallinity values in Table 6.1 [27]. Thus, the peak around 22.5° has been broadened accompanied by a decrease in the relative intensity until SMAF 0.7.

Further addition of 0.8wt% of NH_4HCO_2 salt has decreased the amorphous nature of the sample SMAF 0.8. Hence, the bio-electrolyte SMAF 0.7 has the most amorphous peak with a relatively low peak intensity compared to all the prepared samples. This favours the ease of ionic migration due to the distortion in the biopolymer backbone of SGBP, thus enabling high conductivity for the maximum amorphous sample SMAF 0.7. The decrease in the amorphous nature of the membrane SMAF 0.8 has been explained by the fact that the host matrix SGBP can no longer accommodate the ionic dopant and hence excess salt forms inert ion pairs on the surface causing an increase in crystalline nature to the bio-electrolyte SMAF 0.8 as in Table 6.1 [26].

6.1.3 *Fourier Transform InfraRed Spectroscopy (FTIR)*

6.1.3.1 *FTIR for magnesium chloride doped SG bio-electrolyte SGMC 0.7*

The FTIR spectra for the *Salmalia Malabarica* Gum (SG) and its blend with PVA – SGBP (1g SG + 0.8g PVA) are shown in Figures 6.9 and 6.10. In pure SG the peak corresponding to – OH stretching is relatively low intensity when compared to the SGBP membrane as tabulated in Table 6.2. This increase in intensity for the – OH stretching may be due to the interaction of the functional groups in the SG and PVA [17]. This band is shifted to 3327 cm^{-1}, 3321 cm^{-1}, 3327 cm^{-1}, and 3327 cm^{-1} for all the prepared bio-electrolytes SGMC 0.5, SGMC 0.6, SGMC 0.7, and SGMC 0.8 respectively in Figure 6.11.

The band at 1606 cm^{-1} and 1205 cm^{-1} and 1147 cm^{-1} were assigned to the C – C ring stretching vibrations, C – O stretching vibrations of the polyols in the biomaterial, and C – O bending vibrations of the polysaccharide rings[28,29] for the SG in Figure 6.9 and similar bands are also observed for SGBP membrane at 1623 cm^{-1}, 1027cm^{-1}. The peak observed at 1205 cm^{-1} in SG was not present in the biopolymer membrane and its electrolytes. This also provides a shred of evidence for the integration of the magnesium chloride salt with the – OH group of the biomaterial SG.

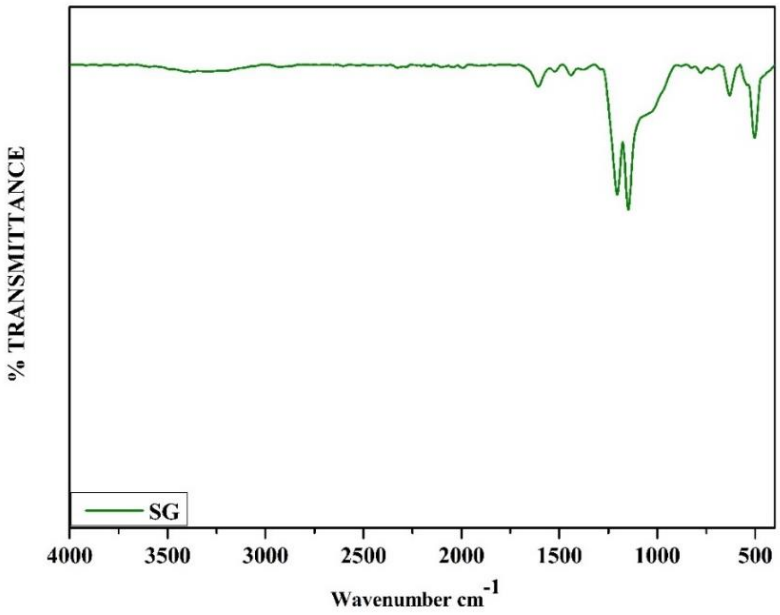

Figure 6.9: FTIR spectra of SG

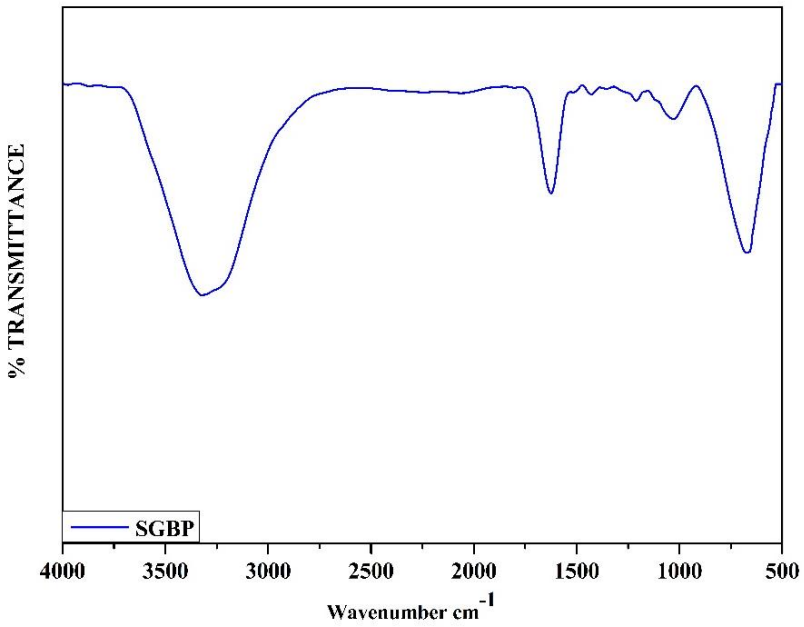

Figure 6.10: FTIR spectra of SGBP (1g SG + 0.8g PVA)

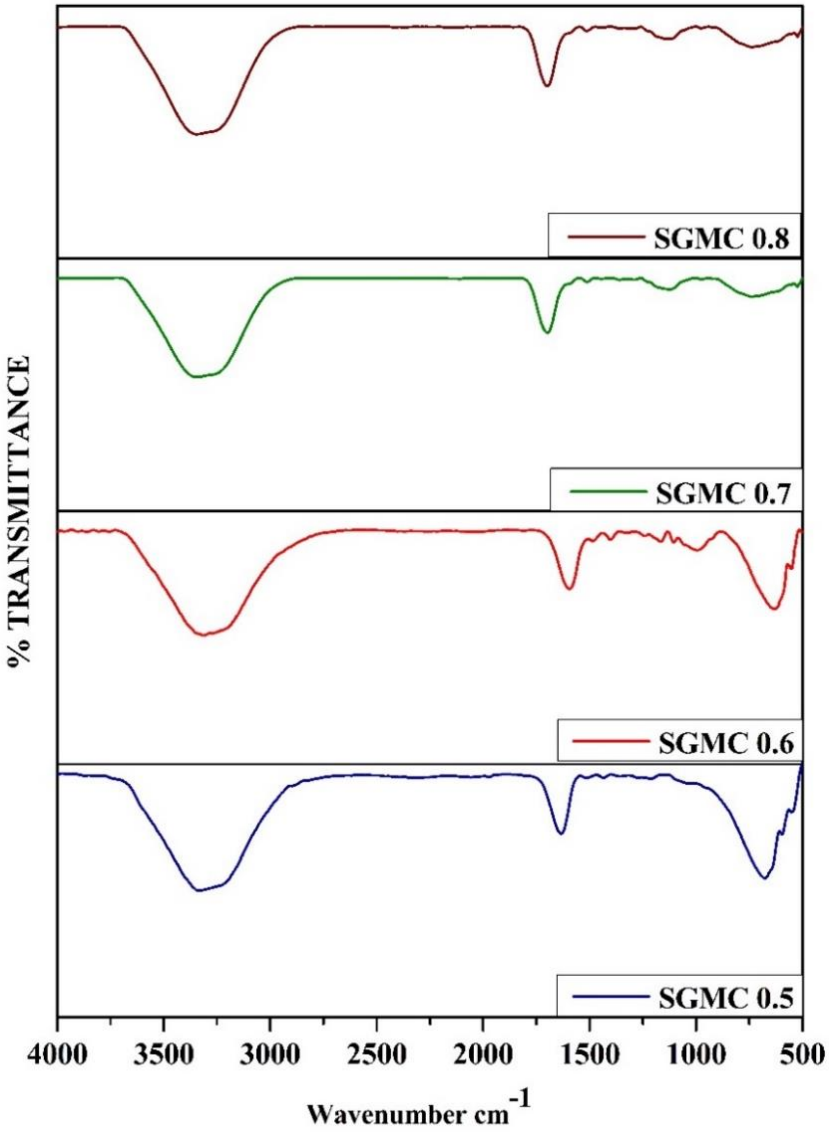

Figure 6.11: FT – IR spectra of SGMC 0.5, SGMC 0.6, SGMC 0.7, and SGMC 0.8

The presence of a peak at 630 cm^{-1} in SG due to the C – OH bending of the glycosidic linkage has shifted to 667 cm^{-1} in the SGBP membrane [30]. This peak has been observed at 676 cm^{-1}, 680 cm^{-1}, 645 cm^{-1}, and 646 cm^{-1} for the C – OH bending in respective bio-electrolytes [31,32]. The vibrational band equivalent to SG and SGBP for C – C ring stretching vibrations are also observed for all the bio-electrolytes SGMC 0.5 (1633 cm^{-1}), SGMC 0.6 (1629 cm^{-1}), SGMC 0.7 (1633 cm^{-1}), and SGMC 0.8 (1633 cm^{-1}) as given in Table 6.2.

Assignments	SG (in cm^{-1})	SGBP (1g SG + 0.8g PVA) (in cm^{-1})	SGBP + 0.5 wt% $MgCl_2$ (in cm^{-1})	SGBP + 0.6 wt% $MgCl_2$ (in cm^{-1})	SGBP + 0.7wt%$MgCl_2$ (in cm^{-1})	SGBP + 0.8 wt%$MgCl_2$ (in cm^{-1})
–OH stretching	3407	3325	3327	3321	3327	3327
C – C Ring stretching vibrations	1606	1623	1633	1629	1633	1633
– C – O group in polyols in the extract	1205	-	-	-	-	-
C–O stretching of the the **acetyl group of PVA**	1147	1027	1027	1037	1046	1048
C – OH bending of glycosidic linkage	630	667	676	680	645	646

Table 6.2: Peak position and vibrational Assignments of SG, SGBP (1g SG + 0.8g PVA) and SGBP + different concentrations of $MgCl_2$

The peak appeared at 1027 cm^{-1} in SGBP due to the C – O symmetric stretching vibrations shifted to higher wavelengths in the prepared bio-electrolytes to 1027 cm^{-1}, 1037 cm^{-1}, 1046 cm^{-1}, and 1048 cm^{-1} with the increase in addition of magnesium chloride [33]. Hence this shift in wavelength with the incorporation of the salt into the host matrix SGBP confirms the complex formation of the biopolymer membrane with the magnesium chloride salt [34]. These results confirm the complexation of the SG, PVA, and the added magnesium chloride salt.

6.1.3.2 *FTIR for lithium chloride doped SG bio-electrolyte SGLC 0.5*

The changes in the vibration frequencies of the lithium chloride incorporated bio-electrolyte membranes are investigated by the FTIR technique with knowledge of the complex formation between the host matrix SGBP and LiCl. Figure 6.12 shows the infrared spectrum of the bio-electrolytes SGLC 0.3, SGLC 0.4, SGLC 0.5, and SGLC 0.6 respectively.

The observed vibrational frequencies and their assignments for all the prepared membranes have been listed in Table 6.3. The band at 3325 cm^{-1} equivalent to – OH stretching as observed in SGBP film has also been seen at 3341 cm^{-1}, 3361 cm^{-1}, 3363 cm^{-1}, and 3369 cm^{-1} in SGLC 0.3, SGLC 0.4, SGLC 0.5, and SGLC 0.6 respectively. This may be associated with the vibrations of the hydroxyl functional groups interlinked with the hydrogen bonding of the molecules in the SG [35,36]. The vibrational band at 1623 cm^{-1} corresponding to the C – C ring stretching of the various polyols present in the biomaterial SG are seen in the SGBP membrane in Figure 6.10 are shifted to 1608 cm^{-1}, 1617 cm^{-1}, 1631 cm^{-1}, and 1633 cm^{-1} respectively [28,29].

The peak at 1429 cm^{-1} seen in SGBP for CH_2 bending vibrations is shifted to higher wavelengths at 1441 cm^{-1}, 1441 cm^{-1}, 1460 cm^{-1}, and 1448 cm^{-1} for the lithium chloride dopped bio-electrolytes in Figure 6.12 [37,38]. The – C – O group stretching vibration for the acetyl group of PVA has been assigned to 1027 cm^{-1} in the SGBP membrane and has seen shifted to higher wavelengths in all the bio-electrolytes. Thus, the decrease in the intensity of the O – H stretching vibrations also supports the complexation between the host matrix and LiCl and the shift in the vibrational frequencies of the peaks in the spectra also evidence the integration of the host and the salt [23].

Table 6.3: Peak position and vibrational Assignments of the bio-membrane and bio-electrolytes SGLC 0.3, SGLC 0.4, SGLC 0.5, and SGLC 0.6 with different concentrations of LiCl salt.

Assignments	SGBP (in cm^{-1})	SGLC 0.3 (in cm^{-1})	SGLC 0.4 (in cm^{-1})	SGLC 0.5 (in cm^{-1})	SGLC 0.6 (in cm^{-1})
–OH stretching	3325	3341	3361	3363	3369
C – C Ring stretching vibrations	1623	1608	1617	1631	1633
CH_2 bending	1429	1441	1441	1460	1448
– C – O group in the **acetyl group of PVA**	1027	1029	1031	1031	1033

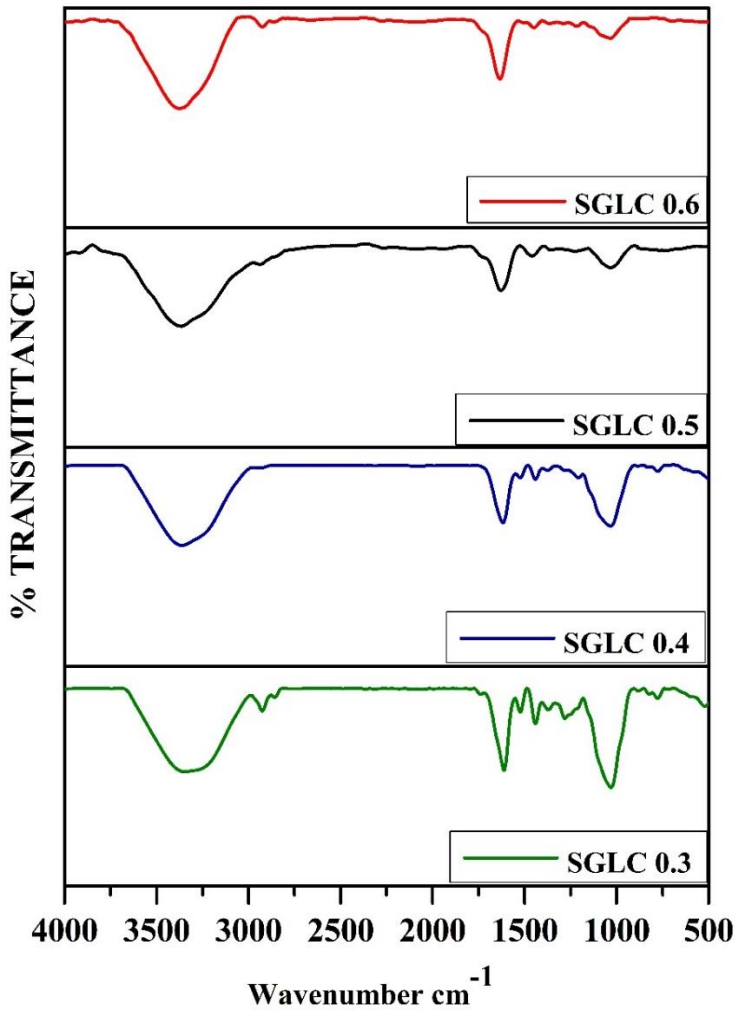

Figure 6.12: FTIR spectra of SGLC 0.3, SGLC 0.4, SGLC 0.5, and SGLC 0.6

6.1.3.3 *FTIR for ammonium formate doped SG bio-electrolyte SGAF 0.7*

The FTIR spectra for the ammonium formate incorporated bio-electrolytes are graphically represented in Figure 6.13. The broadening or shifting of the peaks along with the appearance and disappearance of peaks helps to confirm the complexation of the added salt with the host matrix [27].

In the present work, the stretching vibration for the hydroxyl group occurs at 3341 cm^{-1}, 3361 cm^{-1}, 3363 cm^{-1}, and 3369 cm^{-1} for SMAF 0.5, SMAF 0.6, SMAF 0.7, and SMAF 0.8 respectively as given in Table 6.4. The shift in this band to higher wavelengths and the change in relative intensity affirms the integration of the salt with the host matrix SGBP since the conduction in the bio-electrolyte takes place via the – OH group present in the SG/PVA blend (SGBP) [39,40]. Typically, an ammonium dopant, has H^+ originating from the ionic dopant and is the contributing species for the ionic conductivity of the electrolyte.

Table 6.4: Peak position and vibrational Assignments of the bio-membrane and bio-electrolytes SGAF 0.5, SGAF 0.6, SGAF 0.7, and SGAF 0.8 with different concentrations of NH_4HCO_2 salt

Assignments	SGBP (in cm^{-1})	SGAF 0.5 (in cm^{-1})	SGAF 0.6 (in cm^{-1})	SGAF 0.7 (in cm^{-1})	SGAF 0.8 (in cm^{-1})
–OH stretching	3325	3341	3361	3363	3369
C – C Ring stretching vibrations	1623	1608	1617	1631	1633
CH_2 bending	1429	1441	1441	1460	1448
– C – O group in the **acetyl group of PVA**	1027	1029	1031	1031	1033
C – C stretching	-	817	811	858	844

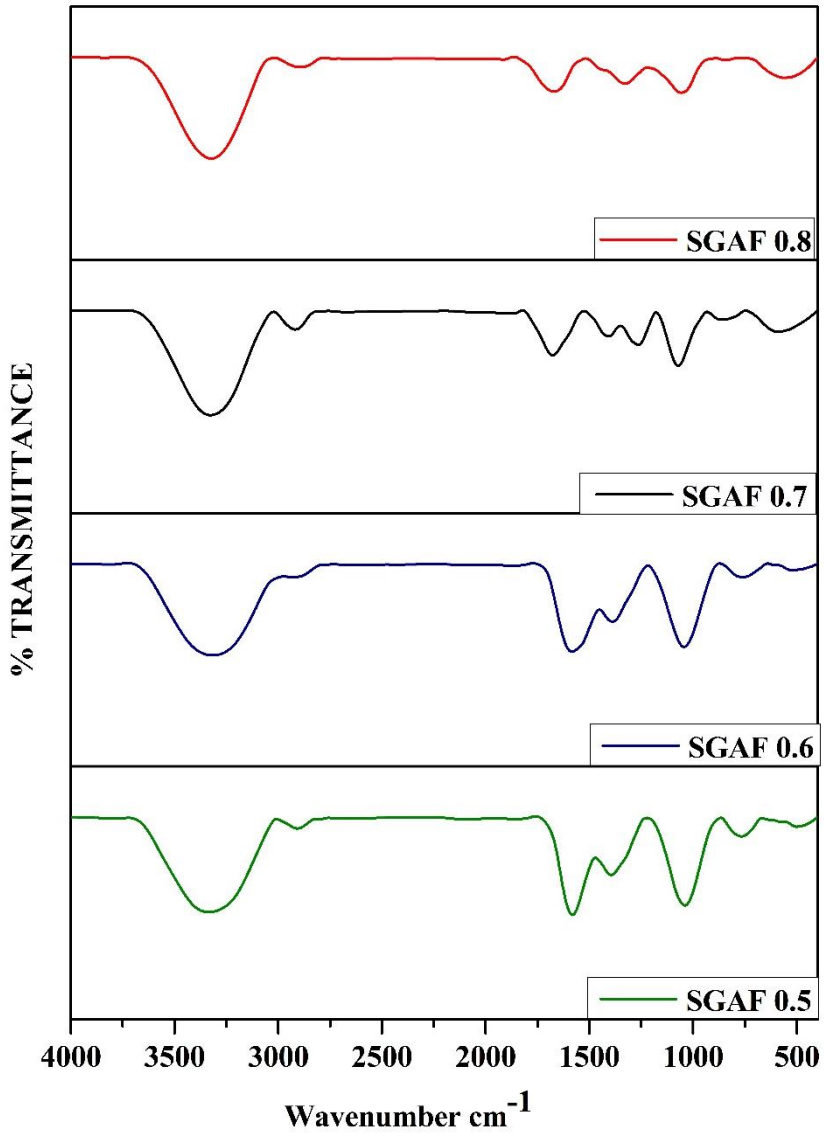

Figure 6.13: FTIR spectra of SGAF 0.5, SGAF 0.6, SGAF 0.7, and SGAF 0.8

Further, the band for the – C – O group in the acetyl group of PVA appeared at 1027 cm^{-1} in the SGBP membrane, but there is a change in relative intensity with the increase in salt concentration. This band has been shifted to 1029 cm^{-1}, 1031 cm^{-1}, 1031 cm^{-1}, and 1033 cm^{-1} in all the doped bio-electrolytes indicating the complexation of the salt with the host [41]. Also, the peaks at 817 cm^{-1}, 811 cm^{-1}, 858 cm^{-1}, and 844 cm^{-1} for C – C stretching in the respective bio-electrolytes SGAF 0.5 to SGAF 0.8 are due to the CH_2 stretching vibrations of the glycosidic groups in the blend SGBP [42,43].

The changes to the vibrational bands of the bio-electrolytes thus help to confirm the complexation of the ionic dopant, the biomaterial SG, and the PVA.

6.1.4 *Differential Scanning Calorimetry (DSC)*

6.1.4.1 DSC for magnesium chloride doped SG bio-electrolyte SGMC 0.7

The thermal behaviour of the samples has been characterized with the differential scanning calorimetry technique by measuring the change in heat capacity of the membrane when they undergo a phase change from a glassy to a rubbery state. This temperature called glass transition temperature (T_g) is associated with the structure and association of the molecules in the membrane composition [44,45]. The glass transition temperature (T_g) of SG and its blend biopolymer membrane SGBP is shown in Figures 6.14 and 6.15. Similarly, the T_g for all the magnesium chloride dopped bio-electrolytes is given in Figure 6.16. The obtained glass transition temperatures for SG, SGBP, and the bio-electrolytes SGMC 0.5, SGMC 0.6, SGMC 0.7, and SGMC 0.8 are listed in Table 6.5. The T_g for the SG is measured to be 50.88°C. From Figure 6.15, it was evident that blending of PVA to the pure SG has increased the T_g to 57.02°C. This may be due to the intermolecular and intramolecular interaction which reduces the fragmental movement of the host biopolymer matrix SGBP which distorts the free rotation of the segments and decreases the flexibility of the prepared membrane SGBP. This causes the glass transition to increase with the addition of polyvinyl alcohol in Figure 6.15 [46,47].

With the further addition of dopant in the SGBP composition, it was observed that there is a decline in glass transition temperature for SGMC 0.5, SGMC 0.6, and SGMC 0.7 corresponding to 0.5wt%, 0.6wt%, and 0.7wt% addition of magnesium chloride. The decrease in the T_g value indicates that the ionic dopant acts as a plasticizer for the host matrix up to 0.7wt% $MgCl_2$ addition. The presence of the $MgCl_2$ in the SGBP host distorts its ordered arrangement between the biopolymer backbone and reduces the transient cross-linkage which in turn reduces the T_g value [48]. This brings good flexibility to the membrane along with good ionic mobility and thus the bio-electrolyte SGMC 0.7 with low T_g among the prepared membrane possesses the highest ionic conductivity s given in Table 6.5. The high amorphous nature of the SGMC 0.7 membrane in XRD also supports these results [49,50].

Table 6.5: Glass transition temperature of Pure SG, SGBP and SGBP with different concentrations of $MgCl_2$, LiCl, and NH_4HCO_2

COMPOSITION	T_g
SG	**50.88°C**
SGBP (1g SG + 0.8g PVA)	**57.02°C**
Magnesium chloride – doped SGBP bio-electrolytes	
SGBP + 0.5wt% $MgCl_2$	45.37°C
SGBP + 0.6wt% $MgCl_2$	40.46°C
SGBP + 0.7wt% $MgCl_2$	**35.59°C**
SGBP + 0.8wt% $MgCl_2$	43.96°C
Lithium chloride – doped SGBP bio-electrolytes	
SGBP + 0.3wt% LiCl	64.48°C
SGBP + 0.4wt% LiCl	43.36°C
SGBP + 0.5wt% LiCl	**33.25°C**
SGBP + 0.6wt% LiCl	45.87°C
Ammonium formate – doped SGBP bio-electrolytes	
SGBP + 0.5wt% NH_4HCO_2	49.81°C
SGBP + 0.6wt% NH_4HCO_2	44.35°C
SGBP + 0.7wt% NH_4HCO_2	**41.47°C**
SGBP + 0.8wt% NH_4HCO_2	48.40°C

Besides all these facts, the addition of 0.8wt% of $MgCl_2$ to the SGBP composition increases the T_g value for SGMC by 0.8. This is explained that the magnesium ions form ion aggregates which reduce the ionic mobility and make the membrane rigid [34,51] hence T_g value increases. Hence from the DSC results, the bio-electrolyte with the lowest T_g as listed in Table 6.5 possess high amorphous nature as supported by the X-ray diffraction technique which is in good agreement.

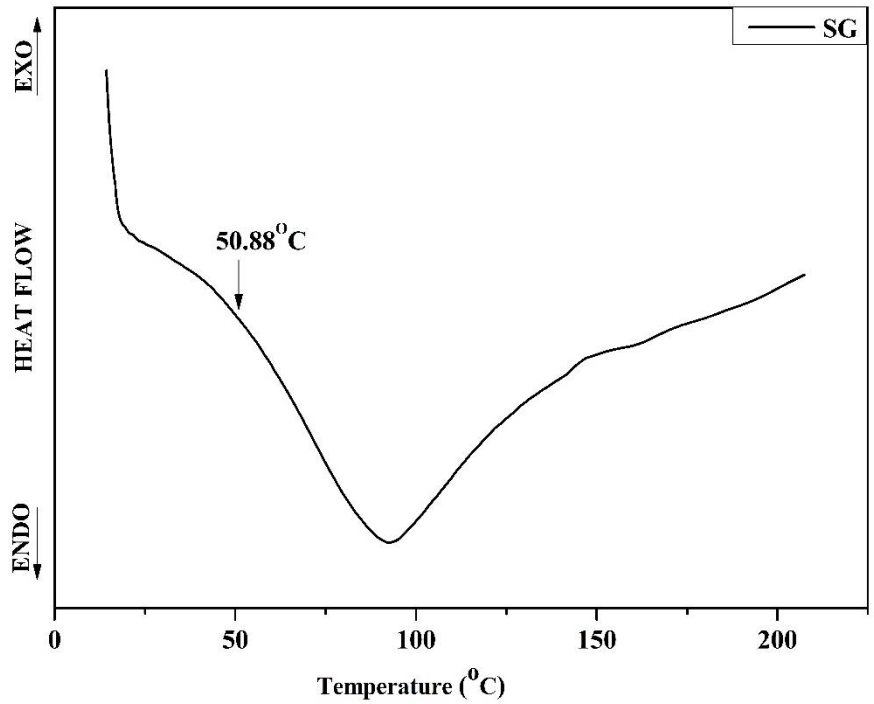

Figure 6.14: DSC thermogram of SG

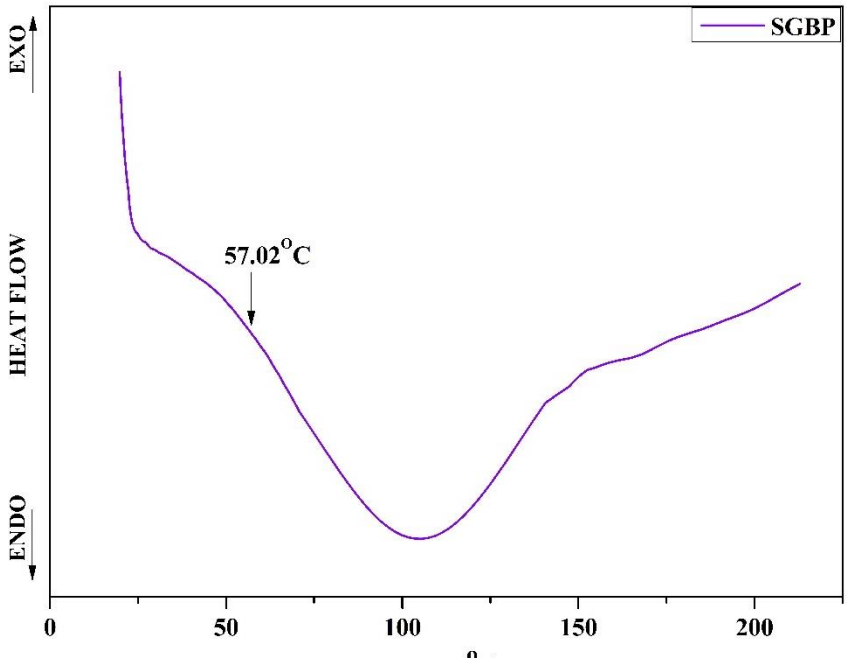

Figure 6.15: DSC thermogram of SGBP (1g SG + 0.8g PVA)

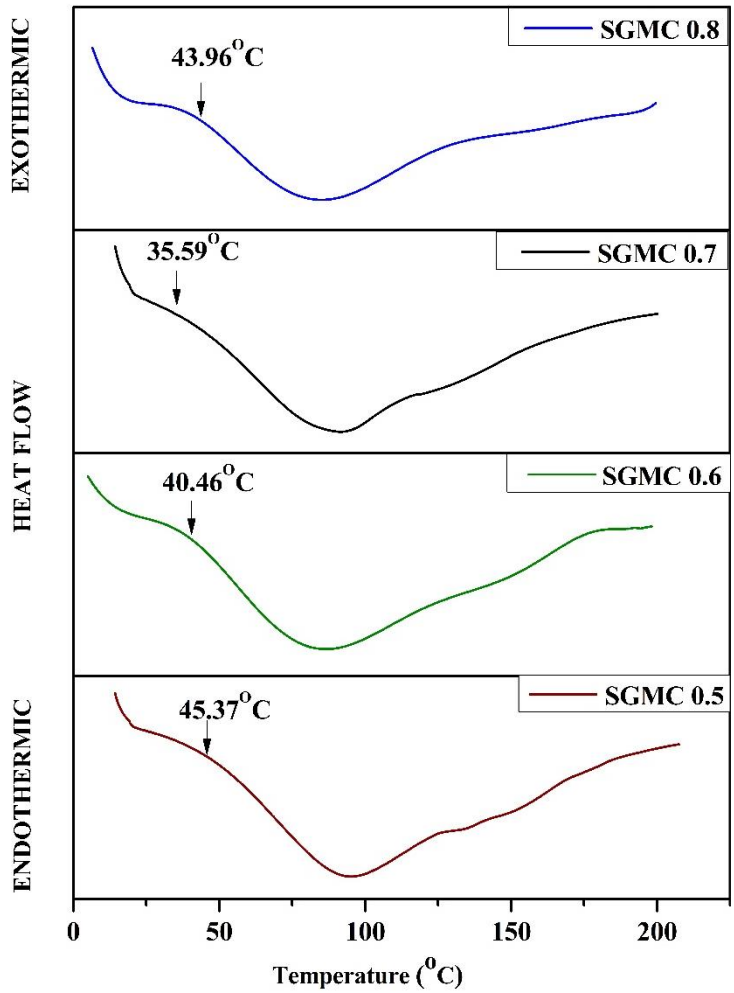

Figure 6.16: DSC thermogram of SGMC 0.5, SGMC 0.6, SGMC 0.7, and SGMC 0.8

6.1.4.2 *DSC for lithium chloride doped SG bio-electrolyte SGLC 0.5*

DSC thermograms have been measured for the lithium chloride incorporated bio-electrolytes SGLC 0.3, SGLC 0.4, SGLC 0.5, and SGLC 0.6 as portrayed in Figure 6.17. With the incorporation of the ionic dopant, lithium chloride into the host matrix SGBP, the T_g values of the bio-electrolyte initially increased for SMLC 0.3 and then shows a depreciation as listed in Table 6.5. The initial increase in the glass transition value may be attributed to the inter and intra-molecular bonding between the added Li^+ ion and the hydroxyl groups of the host composition [46,52]. This interaction causes a strong transient cross-linkage and declines the fragmental motion of the segments of the host matrix [53]. But with further increase in the

concentration of the salt decreases the T_g value up to 0.5wt% concentration after which there is an increase in the transition temperature for 0.6wt% i.e., SMLC 0.6 as depicted in Figure 6.17. An increase of the dopant in the biopolymer membrane SGBP composition, causes a plasticizing effect on the membrane, thereby increasing its flexibility.

The lower the T_g value, the higher the flexibility of the membrane which in turn higher the ionic conductivity of the bio-electrolyte membrane [54,55]. Thus SMLC 0.5 bio-electrolyte with its lowest T_g value has the highest ionic conductivity with its high flexibility. But the latter increase in T_g has been explained by the fact of formation of ionic aggregates of the excess lithium chloride which now can no longer act as transient cross-linkers and reduces the flexibility by enhancing the energy barrier for the fragmental motion of the host matrix SGBP [56,57].

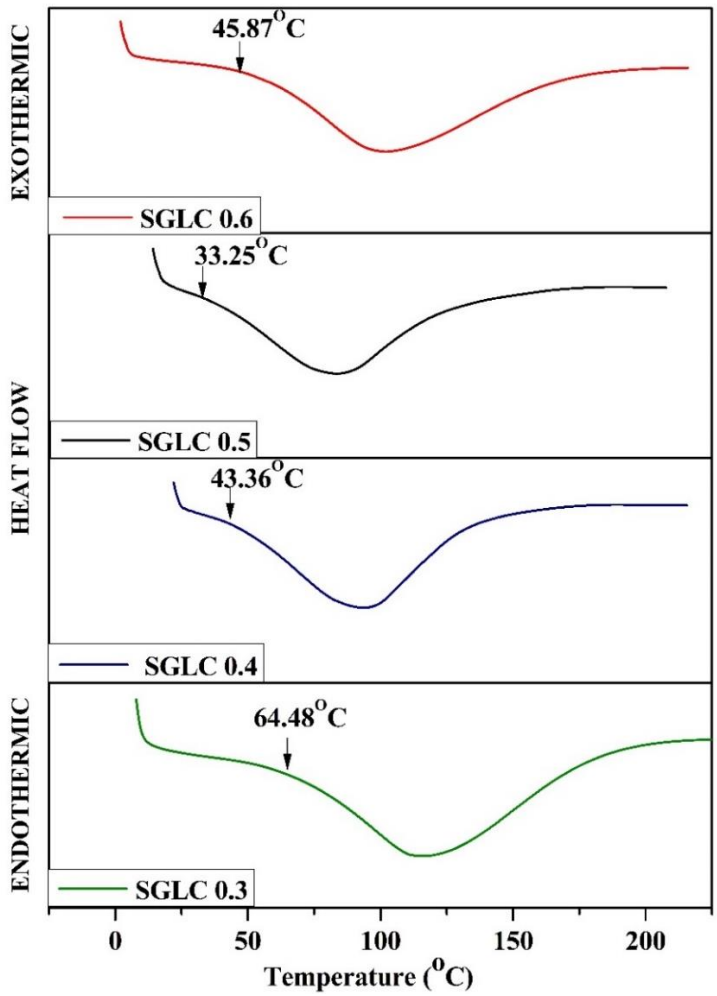

Figure 6.14: DSC thermogram of SGLC 0.3, SGLC 0.4, SGLC 0.5, and SGLC 0.6

6.1.4.3 *DSC for ammonium formate doped SG bio-electrolyte SGLC 0.5*

DSC thermograms for the ammonium formate doped samples SMAF 0.5, SMAF 0.6, SMAF 0.7, and SMAF 0.8 are depicted in Figure 6.18. The variation of the T_g value of the bio-electrolyte has been observed to be dependent on the concentration of the dopant as provided in Table 6.5.

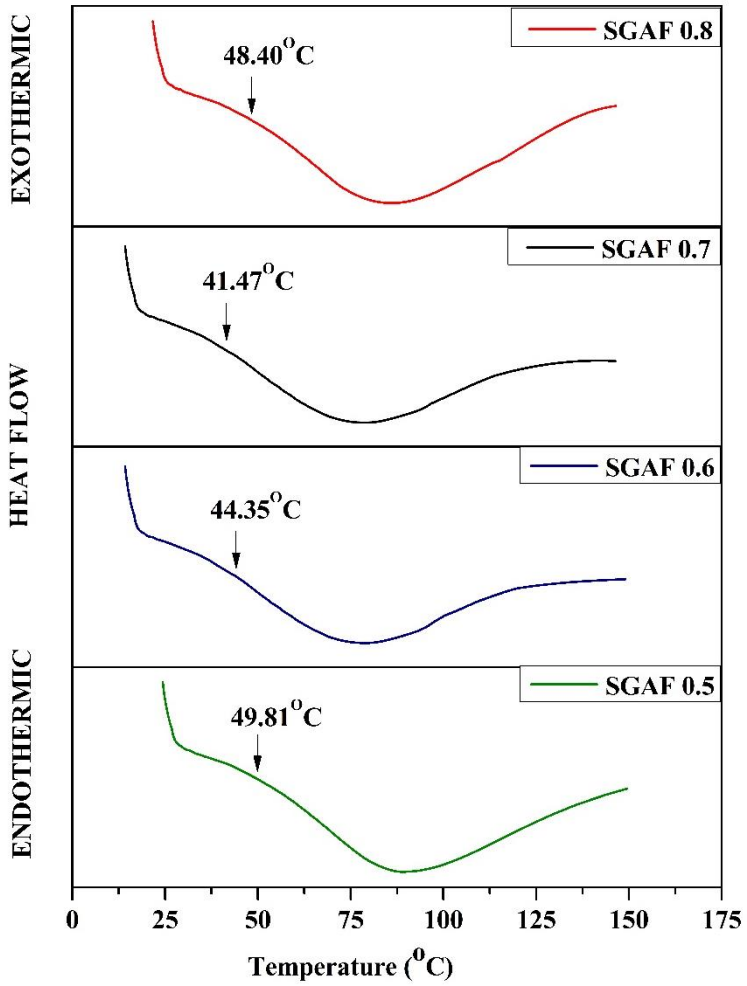

Figure 6.18: DSC thermogram of SGAF 0.5, SGAF 0.6, SGAF 0.7, and SGAF 0.8

The incorporation of ammonium formate of 0.5wt% has a T_g of 49.81°C for SMAF 0.5 which further decreases on increasing the concentration through 0.6wt% and 0.7wt% of NH_4HCO_2 to 44.35°C and 41.47°C. The addition of the dopant helps to plasticize the membrane and reduces the T_g value and enables the membrane more flexible [58] The bio-electrolyte SMAF 0.7 has been found to have the lowest T_g value among the prepared samples

as shown in Table 6.5. The decline in T_g is an indication for the membrane is soft and flexible which enhances the ionic conductivity of the membrane [55]. Thus SGAF 0.7 with the lowest T_g value has the highest amorphous nature which is evidenced by the XRD study and hence will possess the highest ionic conductivity.

Further increase in the concentration of ammonium formate causes an increment in the T_g value for SGAF 0.8 which may be due to the decrease in flexibility of the membrane owing to the excess addition of the salt. The excess salt forms ion aggregates which make the membrane rigid due to the interaction of the salt with the host matrix SGBP [56]. Similar trends have been observed for Moniha et. al., for the iota-carrageenan-based system with ammonium thiocyanate as a dopant [59] and Perumal et.al., for pectin in the lithium chloride-based system [44].

6.1.5 *Linear Sweep Voltammetry (LSV)*

6.1.5.1 *LSV for magnesium chloride doped SG bio-electrolyte SGMC 0.7*

The operational voltage for the energy storage devices such as batteries can be evaluated from the linear sweep voltammetry. This technique is necessary to understand the temperature at which the bio-electrolyte starts to degrade by computing its electrochemical stability window for its application in electrochemical devices [60]. In this regard, the highest conducting bio-electrolyte SGMC 0.7 has been studied for its electrochemical stability window as represented in Figure 6.19.

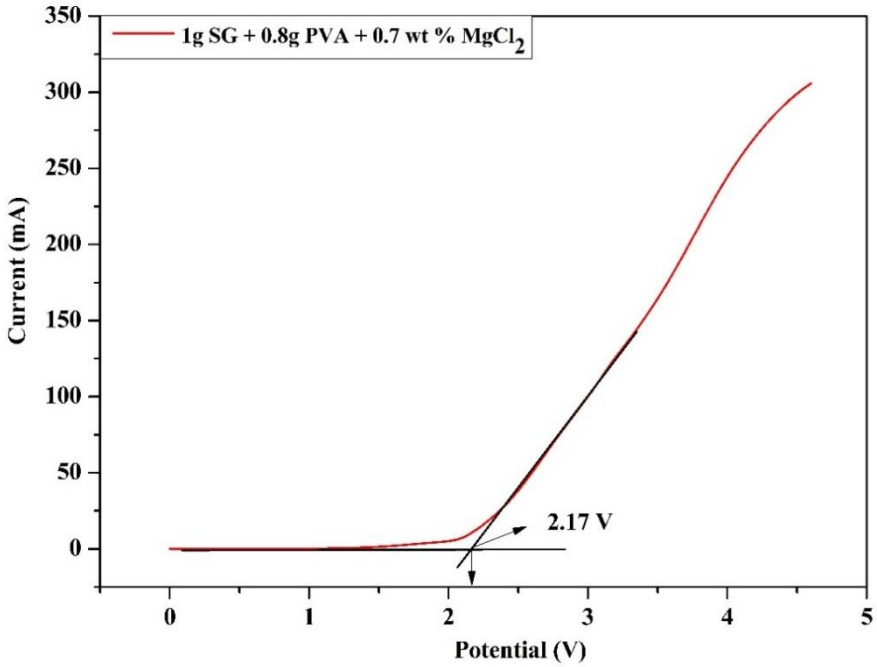

Figure 6.19: LSV plot for the highest Mg-ion conducting SGMC 0.7 bio-electrolyte

It is obvious from Figure 6.19 that the decomposition of the bio-electrolyte SGMC 0.7 occurs beyond 2.17 V after which there is an increase in the current. Comparative results are obtained for Hamsan et al.,[61] using a Chitosan - $MgCl_2$- Glycerol system with an electrode potential stability window of 1.83V and Zainol et al. where PMMA/ Mg $(CF_3SO_3)_2$ electrolyte obtained a potential window of around 2.5 V [62].

6.1.5.2 *LSV for lithium chloride doped SG bio-electrolyte SGLC 0.5*

The electrochemical stability window for the highest conducting bio-electrolyte, SGLC 0.5 has been obtained from Figure 6.20. The LSV plot for SGLC 0.5 membrane starts to decompose after 2.42 V. This provides an insight into the potential window of the cell with SGLC 0.5 membrane as an electrolyte and its applicability in energy storage devices like batteries [60].

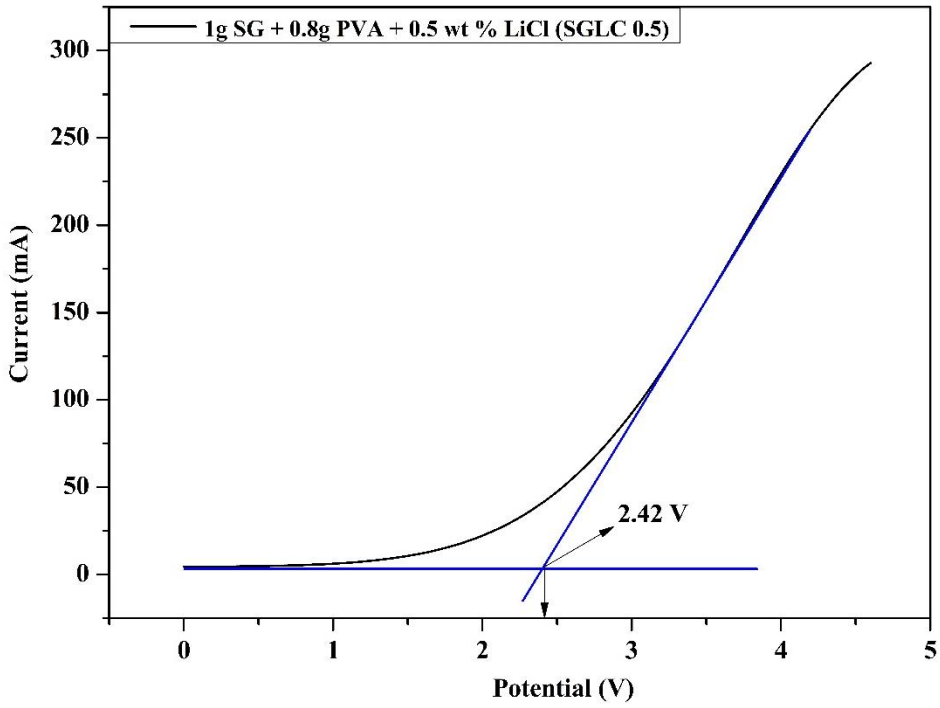

Figure 6.20: LSV plot for the highest Li-ion conducting SGLC 0.5 bio-electrolyte

In the present work, when the potential is increased ahead of 1.1V, the decomposition current increases rapidly initiating the course of an electrochemical reaction in the bio-electrolyte [63].

Leenachandra et.al., was able to study the PVAc-PMMA-LiCl blend as an electrolyte and added plasticizer ethylene carbonate and titania nanofiller to prepare a polymer electrolyte and the potential window was 1.69V and 2.69 V for (70 wt% PVAc-30 wt% PMMA-0.8% LiCl) and (70 wt% PVAc-30 wt% PMMA-0.8% LiCl- 6 mg TiO_2) [64] and in the work of Aziz et.al., CS-glycerol-Mg $(CH_3COO)_2$-Ni polymer electrolyte synthesized had an electrochemical stability window of 2.4 V [65].

6.1.5.3 *LSV for ammonium formate doped SG bio-electrolyte SGLC 0.5*

The electrochemical stability window for the highest conducting bio-electrolyte SGAF 0.7 has been depicted in Figure 6.21. This characterization technique is essential to understand the stability of the bio-electrolyte over a potential variation without degradation. As the potential is swept up to 1.2 V the bio-electrolyte produces a steady current. Later, due to the electrochemical reaction, the membrane degrades after 2.01 V.

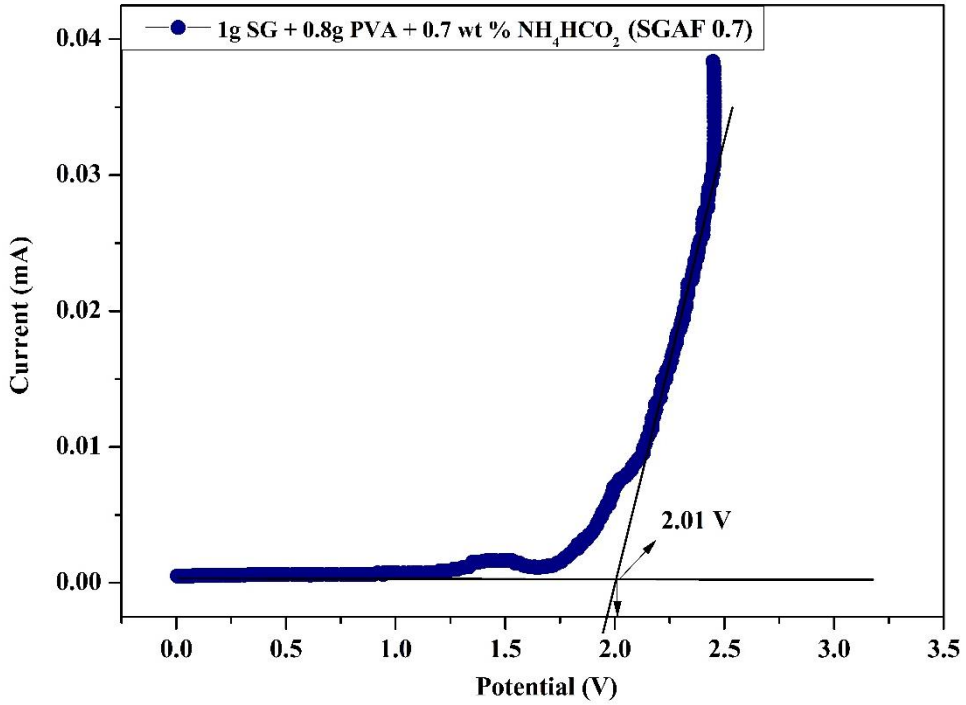

Figure 6.21: LSV plot for the highest proton conducting SGAF 0.7 bio-electrolyte

Thus, the working potential for the 1g SG + 0.8g PVA + 0.7wt% NH_4HCO_2 (SGAF 0.7) membrane is 2.01 V. Similar results as 2.3V has been observed for Aziz et.al., for the PEO/polyvinyl pyrrolidone blend polymer electrolyte doped with NH_4F [66]. Marf et.al. reported a potential range of 1.3 V for the PVA: CS-based proton conducting polymer electrolytes [67].

6.1.6 *Transference Number Measurement (TNM)*

6.1.6.1 *TNM for magnesium chloride doped SG bio-electrolyte SGMC 0.7*

The transference number measurement has been studied to investigate the predominant charge carrier responsible for ionic conductivity in the prepared bio-electrolyte systems. In this work, Wagner's [68] polarization technique is adopted to measure the ion transport number or transference number for the highest conducting SGMC 0.7 bio-electrolyte. This technique operates with a constant DC voltage of 1.5 V across the cell SS|1g SG + 0.8g PVA + 0.7wt% $MgCl_2$|SS, to polarize them, and the variation of current with time has been plotted in Figure 6.22.

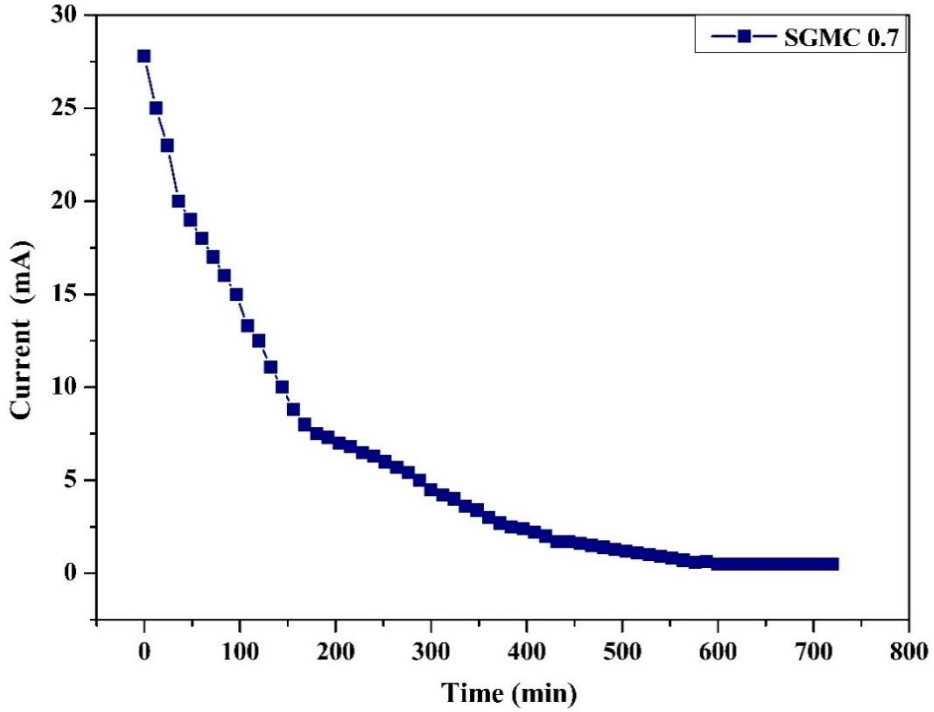

Figure 6.22: Polarisation cure Vs Time of the cell for the highest conducting SGMC 0.7 Mg-ion electrolyte

The transference number has been computed by the formula given in equation 3.3 and equation 3.4 from Chapter 3 [69] and has appeared to be 0.98. This is similar to the report of M.S.A. Rani et.al [70] for a CMC-Mg (20) biopolymer electrolyte system using Mg $(CH_3COO)_2$ as the ionic dopant. Thus, this technique suggests the Mg – ions as the predominant charge carrier in the SGMC 0.7 bio-electrolyte system.

6.1.6.2 *TNM for lithium chloride doped SG bio-electrolyte SGLC 0.5*

The lithium transference numbers have been measured for the highest conducting bio-electrolyte, 1g SG + 0.8g PVA + 0.5wt% LiCl (SGLC 0.5) by the Wagner's polarization technique [68] as discussed earlier. The cationic transference number should be closer to unity to enable the contributing species as ions for the ionic conductivity and prevent the migration of electrons, thus serving the purpose of electrolyte [71]. In this technique, stainless steel blocking electrodes hold the cell by packing the highest conducting SGLC 0.5 electrolyte between them as SS|1g SG + 0.8g PVA + 0.5wt% LiCl| SS. The variation of current is recorded over time as in Figure 6.23.

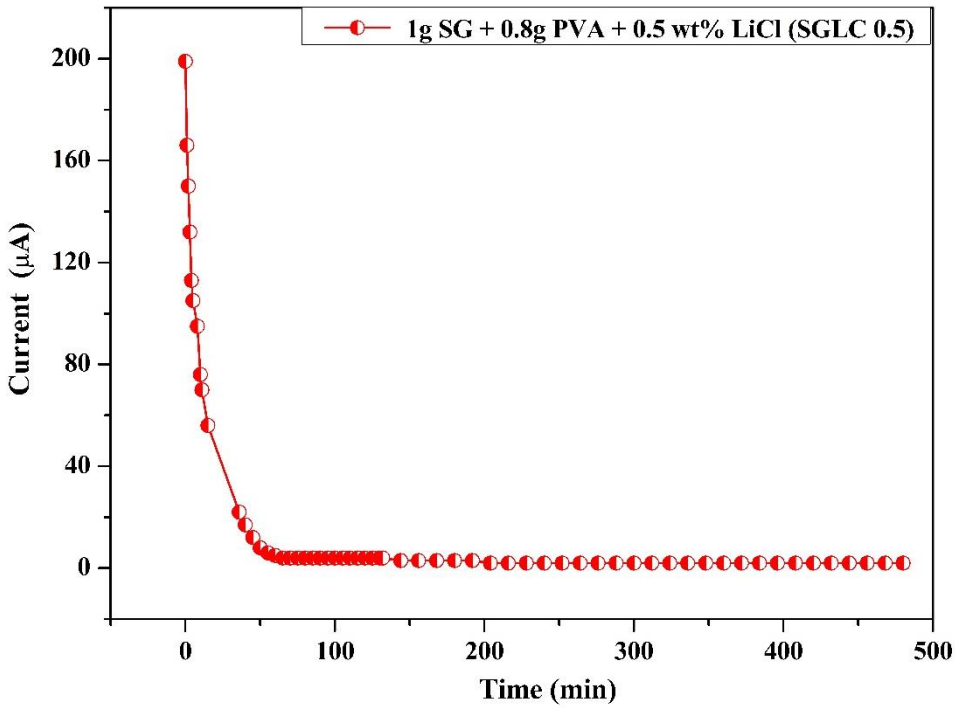

Figure 6.23: Polarisation cure Vs Time of the cell for the highest conducting SGLC 0.5 Li-ion electrolyte

While DC voltage is applied, migration of ions occurs through the SMLC 0.5 bio-electrolyte, and the current decreases till a point where the ions are depleted in the electrolyte, after which a steady flow of current takes place [71]. From the plot in Figure 6.22, the initial (I_i) and final (I_f) currents are noted. Thus, the transference number has been calculated from the formula in equation 3.3 and equation 3.4 as 0.99. This result suggests that the conductivity of the bio-electrolyte is prominently due to the ions and the electron contribution is negligible [72].

6.1.6.3 *TNM for ammonium formate doped SG bio-electrolyte SGAF 0.7*

The ionic transference number for the highest conducting 1g SG + 0.8g PVA + 0.7wt% NH_4HCO_2 (SGAF 0.7) membrane has been obtained from Wagner's polarization technique [73]. The confirmation of the contributing species for the overall conductivity of the SGAF 0.7 bio-electrolyte has been calculated from the plot of polarization current versus time in Figure 6.24.

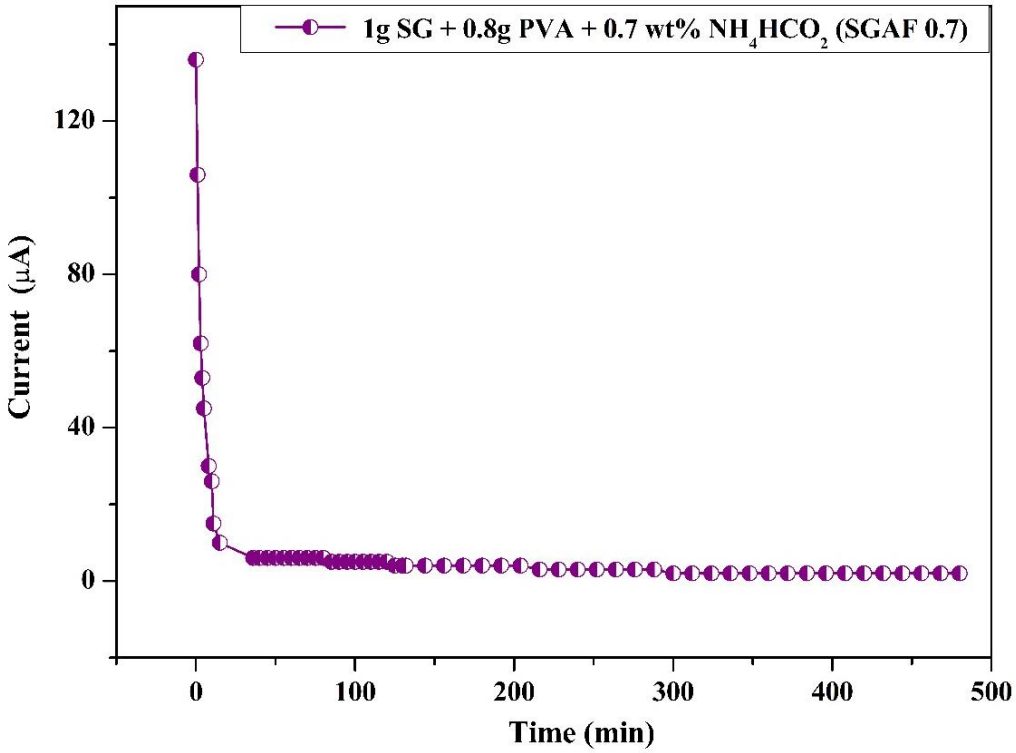

Figure 6.24: Polarization cure Vs Time of the cell for the highest conducting SGAF 0.7 bio- electrolyte

For the computation of TNM, a dc voltage of 1.5 V has been applied across the cell of configuration SS|1g SG + 0.8g PVA + 0.7wt% NH_4HCO_2|SS. The polarization current has been recorded with time, which shows an initial decrease in the current due to the ion migration through the bio-electrolyte. Later, a steady state is reached when the electrolyte is devoid of ions for transport [74]. The ionic transference number of SGAF 0.7 was obtained as 0.98 which has been computed from equations 3.4 and 3.4 as explained in Chapter 3 [69].

6.1.7 *Electrochemical Impedance Spectroscopy (EIS)*

6.1.7.1 *EIS for magnesium chloride doped SG bio-electrolyte SGMC 0.7*

The impedance plot for SG/PVA blend magnesium bio-electrolytes at room temperature with various magnesium chloride concentrations is depicted in Figure 6.25. This impedance analysis is an important characterization technique to analyze the electrochemical properties of the electrolyte films. A typical Nyquist plot comprises of high-frequency

depressed semicircle region and a low-frequency tail or a spike region. The bulk effect of the electrolyte is represented by the depressed semicircle while the inclined spike or tail is due to the blocking effect at the electrode-electrolyte interface [75].

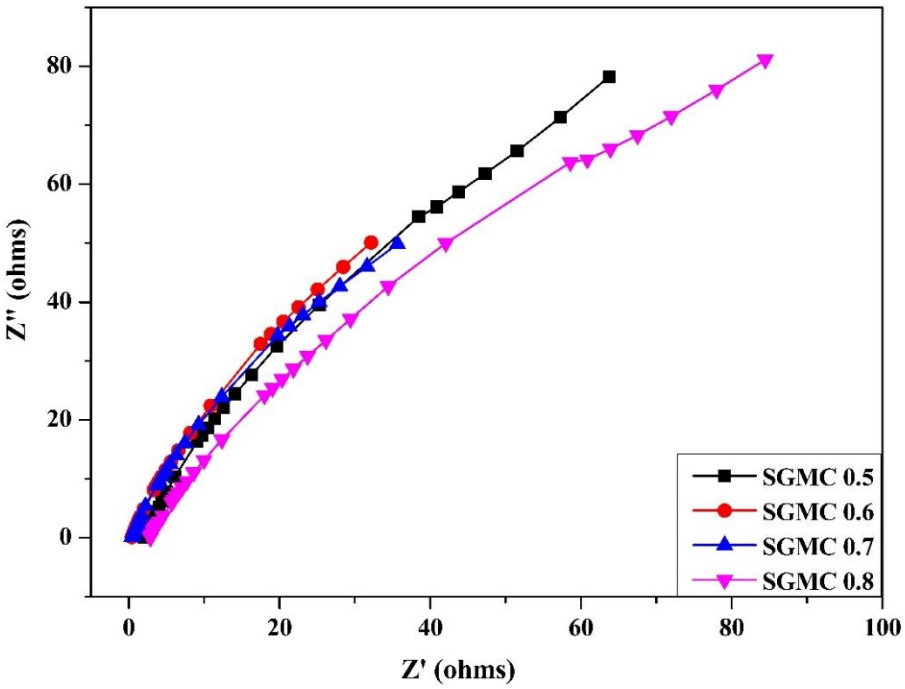

Figure 6.25: Nyquist plot for SGMC 0.5, SGMC 0.6, SGMC 0.7, and SGMC 0.8 at room temperature

In the present work, only an inclined spike has been observed in the impedance plot in Figure 6.25 and the semicircle in the high-frequency region was absent. This is due to the ion accumulation from electrode polarisation at the electrode-electrolyte interface and hence the DC conductivity is due to the migration of ions since the total impedance at the high-frequency region becomes zero due to the absence of the semicircle. This is also evident from Table 6.6 that the bulk resistance R_b decreases with the increase in dopant concentration [75,76]. The R_b values for all the electrolytes are calculated from the EQ software by B. A. Boukamp [77,78]. The ionic conductivity for all the samples has been calculated from equation (3.5) given in Chapter 3.

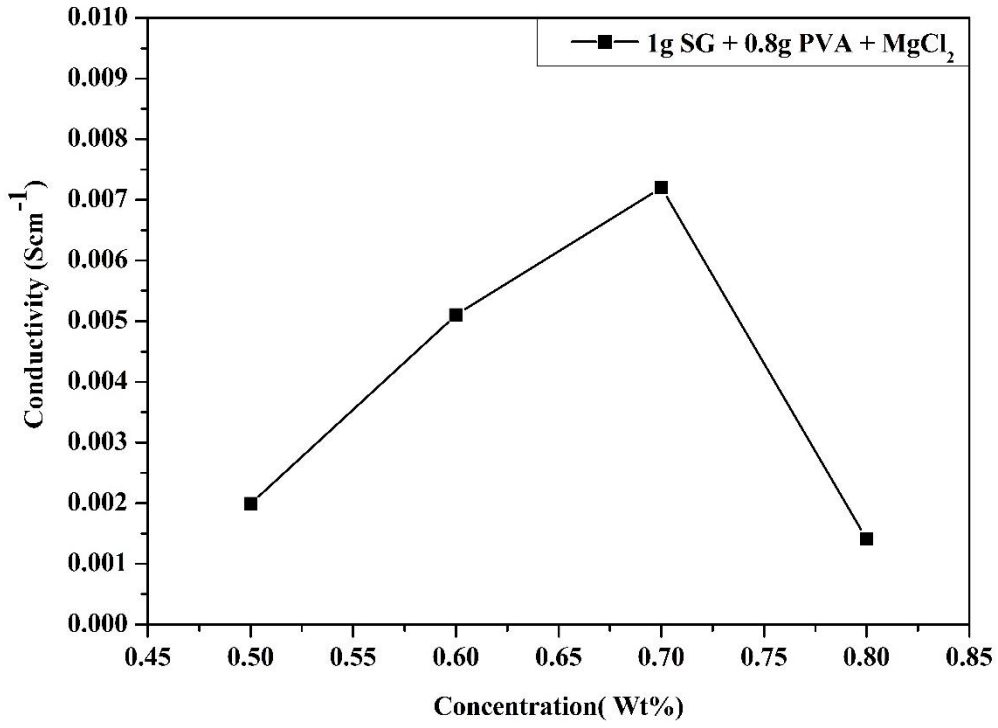

Figure 6.26: Effect of concentration of magnesium chloride on the conductivity of the biopolymer membrane SGBP (1g SG + 0.8g PVA)

The maximum ionic conductivity obtained in the present work is 7.2×10^{-3} S cm^{-1} for the bio-electrolyte SGMC 0.7 as mentioned in Table 6.6. Also, the variation of ionic conductivity with various concentrations of magnesium chloride from 0.5wt% to 0.8wt% at room temperature is plotted in Figure 6.26. The conductivity of the electrolyte system is dependent on the concentration of the carrier ions and their free availability for mobility through the electrolyte [79].

Hence a free ion in a flexible membrane is recommended for the high-conducting membrane which is in good agreement with the present results of DSC studies and XRD analysis [69]. It was SGMC 0.7 with maximum ionic conductivity has the lowest Tg value and possesses high amorphous nature as confirmed by these results in the study. Hence this DC conductivity analysis is proof of the application of these bio-electrolytes for battery applications.

Table 6.6: Ionic conductivity (σ) values of the biopolymer electrolytes at 303K

Composition	σ (S cm^{-1})	R_b (Ω)
SGBP (1g SG + 0.8g PVA)	3.11×10^{-5}	2567
Magnesium chloride – doped SGBP bio-electrolytes		
SGBP + 0.5wt% $MgCl_2$	1.99×10^{-3}	14.11
SGBP + 0.6wt% $MgCl_2$	5.1×10^{-3}	3.31
SGBP + 0.7wt% $MgCl_2$	**7.2×10^{-3}**	**2.72**
SGBP + 0.8wt% $MgCl_2$	1.41×10^{-3}	19.06
Lithium chloride – doped SGBP bio-electrolytes		
SGBP + 0.3wt% LiCl	5.41×10^{-4}	17.5
SGBP + 0.4wt% LiCl	8.78×10^{-4}	16.1
SGBP + 0.5wt% LiCl	**1.39×10^{-3}**	**11.8**
SGBP + 0.6wt% LiCl	8.82×10^{-4}	12.4
Ammonium formate – doped SGBP bio-electrolytes		
SGBP + 0.5wt% NH_4HCO_2	2.09×10^{-3}	14.10
SGBP + 0.6wt% NH_4HCO_2	3.61×10^{-3}	6.00
SGBP + 0.7wt% NH_4HCO_2	**5.33×10^{-3}**	**2.54**
SGBP + 0.8wt% NH_4HCO_2	9.62×10^{-4}	19.68

6.1.7.2 *EIS for lithium chloride doped SG bio-electrolyte SGLC 0.5*

Figure 6.27 interpret the impedance analysis plot for the lithium chloride dopped bio-electrolytes SGLC 0.3, SGLC 0.4, SGLC 0.5, and SGLC 0.6. The Nyquist plots for the pure SG and its blend with PVA i.e., SGBP are illustrated in Figure 3.8 in Chapter 3. In this work, impedance shows only a spike in the low-frequency region and the semicircle to be found at the high-frequency region is absent in Figure 6.27. Similar to the above results, this supports the fact of the contribution of ions to the ionic conductivity of the membranes [80]. From the observed AC impedance measurement data, the ionic conductivity of all the prepared membranes is calculated from the formula in equation (3.5) discussed in Chapter 3. The bulk resistance R_b is measured from the impedance plots using EQ software proposed by B.A.Boukamp [77,78] and are provided in Table 6.6.

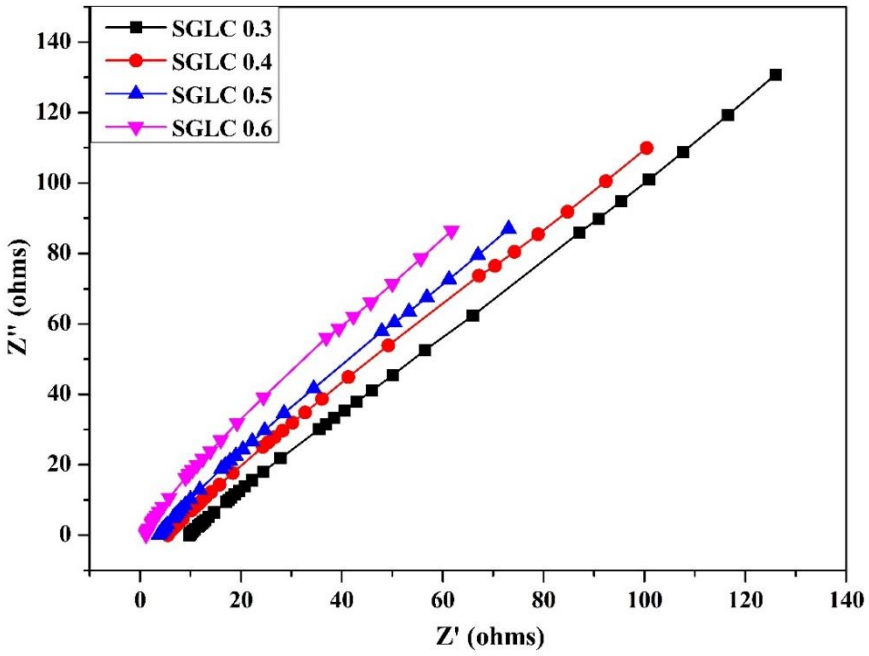

Figure 6.27: Nyquist plot for SGLC 0.3, SGLC 0.4, SGLC 0.5, and SGLC 0.6 at room temperature

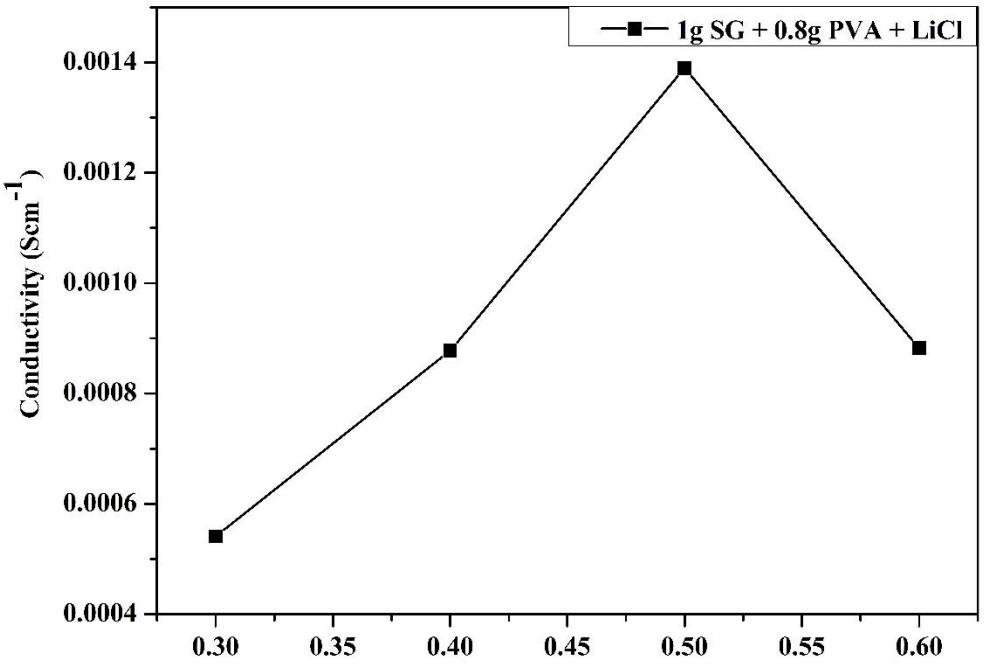

Figure 6.28: Effect of concentration of Lithium Chloride on the conductivity of the biopolymer membrane SGBP (1g SG + 0.8g PVA)

The maximum ionic conductivity of 1.39×10^{-3} Scm^{-1} has been calculated for the bio-electrolyte SMLC 0.5 membrane and the variation of the ionic conductivity with LiCl concentration is plotted in Figure 6.28. The ionic conductivity of the prepared bio-electrolytes appeared to increase with the increase in the concentration of lithium chloride used as an ionic dopant up to SMLC 0.5 after which the addition of 0.6wt% LiCl, caused the decline in the ionic conductivity for the SGLC 0.6 membrane. The increment may be assigned to the introduction of amorphous nature and plasticizing effect with the addition of LiCl to the host matrix. The XRD and DSC results are in good agreement with the above results and SMLC 0.5 has the highest amorphous nature and lowest T_g among all the prepared membranes.

Thus, the more amorphous the membrane eases the migration of ions through the host matrix and hence increases the ionic conductivity [69,79]. But when the tolerance limit of the host matrix SGBP to accommodate the carrier ions has reached, then the conductivity shows a decline. This may be due to the formation of neutral ion pairs by the excess LiCl which hinders the ionic movement through the host surface matrix [81].

6.1.7.3 *EIS for ammonium formate doped SG bio-electrolyte SGAF 0.7*

The impedance measurements are performed to compute the electrical conductivity of the prepared bio-electrolytes SMAF 0.5, SMAF 0.6, SMAF 0.7, and SMAF 0.8 in Figure 6.29. Considering the Nyquist plot in the present work, it has been observed that only a tilted spike at low-frequency owing to the polarization at the electrode-electrolyte interface [66,82]. The absence of the semicircle at high-frequency region indicates the occurrence of a resistance component only and the ionic conductivity of the bio-electrolyte results from the migration of ions [83,84]. The value of bulk resistance (R_b) obtained from the EQ software conceptualized by B. A Boukamp [77,78] and the ionic conductivities computed using the formula in the equation (3.5) for all the prepared samples are provided in Table 6.6.

The ionic conductivity of the bio-electrolytes varies with the increase in the ratio of the added ammonium formate as demonstrated in Figure 6.30 [85]. The ionic conductivity of the un-doped system SGBP was found to be 3.11×10^{-5} S cm^{-1} as in Figure 3.8.

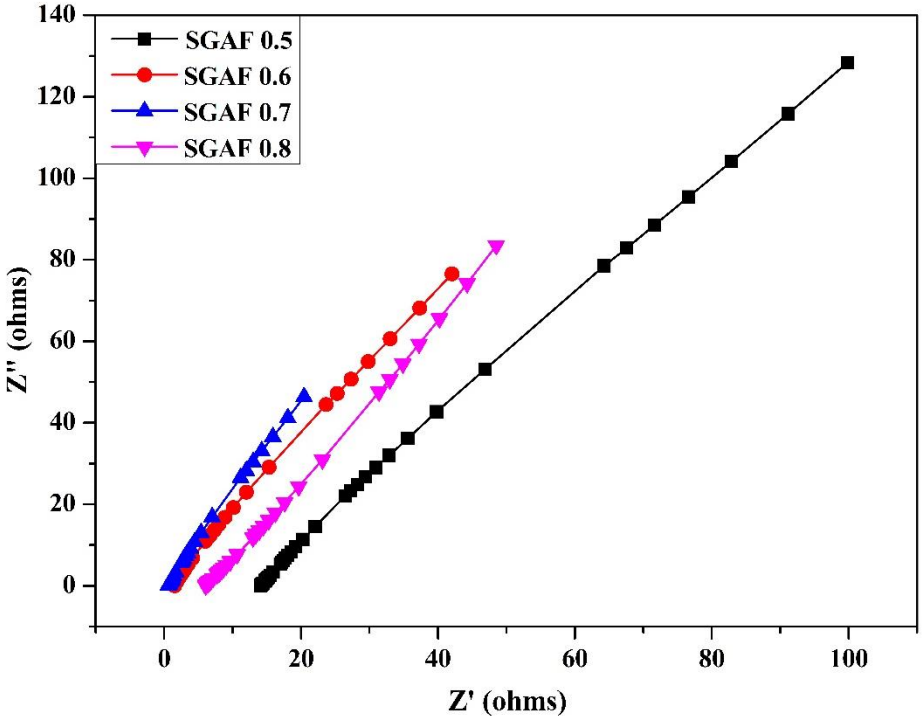

Figure 6.29: Nyquist plot for SGAF 0.5, SGAF 0.6, SGAF 0.7, and SGAF 0.8 at room temperature

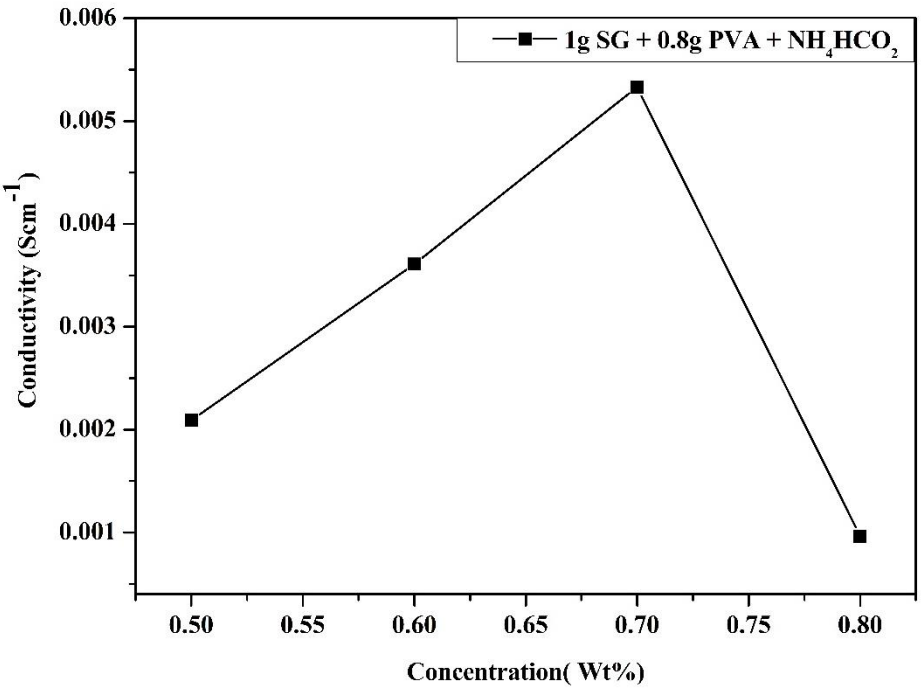

Figure 6.30: Effect of concentration of ammonium formate on the conductivity of the biopolymer membrane SGBP (1g SG + 0.8g PVA)

The addition of the dopant from 0.5 wt% to 0.7wt% increases the ionic conductivity for the membranes SMAF 0.5 to SMAF 0.7. This enhancement may be assigned to the increase in amorphous nature which eases the number of H^+ ions to migrate and integrate with the coordinating site of the host matrix [86,87]. The maximum conductivity has been exhibited by the SMAF 0.7 membrane due to its high amorphous nature as explained in XRD results and high flexibility as confirmed by the DSC study. However, with further addition of salt to 0.8wt%, the ionic conductivity of the SGAF 0.8 show a decline which may be due to the recrystallization of the excess salt which provides an energy barrier for the segmental motion of the host matrix SGBP [88].

References

[1] E.E. Miller, Y. Hua, F.H. Tezel, J Energy Storage 20 (2018) 30–40.

[2] R. Dubey, V. Guruviah, Ionics (Kiel) 25 (2019) 1419–1445.

[3] Z. Niu, H. Dong, B. Zhu, J. Li, H.H. Hng, W. Zhou, X. Chen, S. Xie, Advanced Materials 25 (2013) 1058–1064.

[4] L.F. Aval, M. Ghoranneviss, G.B. Pour, Mater Renew Sustain Energy 7 (2018).

[5] R. Leones, F. Sentanin, L.C. Rodrigues, I.M. Marrucho, J.M.S.S. Esperança, A. Pawlicka, M.M. Silva, Express Polym Lett 6 (2012) 1007–1016.

[6] B. Singh, L. Varshney, S. Francis, Rajneesh, Int J Biol Macromol 88 (2016) 586–602.

[7] Y.H. Ma, J. Yang, B. Li, Y.W. Jiang, X. Lu, Z. Chen, Polym Chem 7 (2016) 2037–2044.

[8] A. Hosseini, S.M. Jafari, H. Mirzaei, A. Asghari, S. Akhavan, Carbohydr Polym 126 (2015) 1–8.

[9] A.K. Shukla, R.S. Bishnoi, M. Kumar, V. Fenin, C.P. Jain, Asian J Pharm Pharmacol 4 (2018) 23–30.

[10] V.D. Prajapati, G.K. Jani, N.G. Moradiya, N.P. Randeria, Carbohydr Polym 92 (2013) 1685–1699.

[11] C. Peng, X. bin Yan, R.T. Wang, J.W. Lang, Y.J. Ou, Q.J. Xue, Electrochim Acta 87 (2013) 401–408.

[12] Li, Jiangfeng, and Qingsheng Wu, *New Journal of Chemistry* 39 (2015): 3859-3864.

[13] T.E. Rufford, D. Hulicova-Jurcakova, Z. Zhu, G.Q. Lu, Electrochem Commun 10 (2008) 1594–1597.

[14] Y. Lv, L. Gan, M. Liu, W. Xiong, Z. Xu, D. Zhu, D.S. Wright, J Power Sources 209 (2012) 152–157.

[15] K. Suvarnna, S.J. Kirubavathy, S. Selvasekarapandian, M.V. Krishna, M. Ramaswamy, Ionics 28 (2022) 1767–1782.

[16] R. Manjuladevi, M. Thamilselvan, S. Selvasekarapandian, R. Mangalam, M. Premalatha, S. Monisha, Solid State Ion 308 (2017) 90–100.

[17] M. Abirami, R. Saratha, R. Shilpa, B. Vinitha, Bulletin of Material Science 43 (2020) 1-6.

[18] R.M. Hodge, G.H. Edward, G.P. Simon, Polymer (Guildf) 37 (1996) 1371–1376.

[19] T.J.R. Reddy, V.B.S. Achari, A.K. Sharma, V.V.R.N. Rao, Ionics (Kiel) 13 (2007) 55–59.

[20] D.V. Pandi, S. Selvasekarapandian, R. Bhuvaneswari, M. Premalatha, S. Monisha, D. Arunkumar, K. Junichi, Solid State Ion 298 (2016) 15–22.

[21] O.G. Abdullah, S.B. Aziz, D.R. Saber, R.M. Abdullah, R.R. Hanna, S.R. Saeed, Journal of Materials Science: Materials in Electronics 28 (2017) 8928–8936.

[22] F.N. Jumaah, N.N. Mobarak, A. Ahmad, M.A. Ghani, M.Y.A. Rahman, Ionics (Kiel) 21 (2015) 1311–1320.

[23] N.N. Mobarak, N. Ramli, A. Ahmad, M.Y.A. Rahman, Solid State Ion 224 (2012) 51–57.

[24] M. Ravi, S. Song, J. Wang, T. Wang, R. Nadimicherla, Journal of Materials Science: Materials in Electronics 27 (2016) 1370–1377.

[25] P.B. Bhargav, V.M. Mohan, A.K. Sharma, V.V.R.N. Rao, Ionics (Kiel) 13 (2007) 173–178.

[26] P. Hu, J. Chai, Y. Duan, Z. Liu, G. Cui, L. Chen, J Mater Chem A Mater 4 (2016) 10070–10083.

[27] M.A. Saadiah, Y. Nagao, A.S. Samsudin, Int J Hydrogen Energy 45 (2020) 14880–14896.

[28] Liu B, Huang Y, Wang J, Li Z, Yang G, Jin S, Iranmanesh E, Hiralal P, Zhou H, RSC Advances 11 (2021) 24862-24871.

[29] S. Karole, G. Gautam, S. Gupta, Asian Journal of Pharmaceutical Education and Research. 6 (2017) 16-27.

[30] R. Md Salim, J. Asik, M.S. Sarjadi, Wood Sci Technol 55 (2021) 295–313.

[31] I.M. de Rosa, J.M. Kenny, D. Puglia, C. Santulli, F. Sarasini, Compos Sci Technol 70 (2010) 116–122.

[32] M. Fan, D. Dai, B. Huang, Fourier Transform- materials analysis 3 (2012) 45-68.

[33] S. Kaidi, Z. Belattmania, F. Bentiss, C. Jama, A. Reani, B. Sabour, Biointerface Res Appl Chem 12 (2022) 6046–6057.

[34] P. Sangeetha, T.M. Selvakumari, S. Selvasekarapandian, S.R. Srikumar, R. Manjuladevi, M. Mahalakshmi, Ionics (Kiel) 26 (2020) 233–244.

[35] K.M. Abd El-Kader, A.S. Orabi, Spectroscopic Behavior of Poly(Vinyl Alcohol) Films with Different Molecular Weights, 2002.

[36] N.X. Chen, J.H. Zhang, Chinese Journal of Polymer Science (English Edition) 28 (2010) 903–911.

[37] S. Keskin, I. Uslu, T. Tunĉ, M. Öztürk, A. Aytimur, Materials and Manufacturing Processes 26 (2011) 1346–1351.

[38] S. Rajendran, M. Sivakumar, R. Subadevi, Mater Lett 58 (2004) 641–649.

[39] M. Hema, S. Selvasekerapandian, G. Hirankumar, A. Sakunthala, D. Arunkumar, H. Nithya, Journal of Physics and Chemistry of Solids 70 (2009) 1098–1103.

[40] M. Hema, S. Selvasekerapandian, A. Sakunthala, D. Arunkumar, H. Nithya, Physica B Condens Matter 403 (2008) 2740–2747.

[41] M. Muthukrishnan, C. Shanthi, S. Selvasekarapandian, G. Shanthi, L. Sampathkumar, T. Maheshwari, Ionics (Kiel) 27 (2021) 3443–3459.

[42] S. Karthikeyan, S. Selvasekarapandian, M. Premalatha, S. Monisha, G. Boopathi, G. Aristatil, A. Arun, S. Madeswaran, Ionics (Kiel) 23 (2017) 2775–2780.

[43] C.S. Ramya, S. Selvasekarapandian, T. Savitha, in: Journal of Solid State Electrochemistry, 2008, 807–814.

[44] P. Perumal, P. Christopher Selvin, S. Selvasekarapandian, Ionics (Kiel) 24 (2018) 3259–3270.

[45] X. Li, H. Xie, J. Lin, W. Xie, X. Ma, Polym Degrad Stab 94 (2009) 1–6.

[46] G. Nirmala Devi, S. Chitra, S. Selvasekarapandian, M. Premalatha, S. Monisha, J. Saranya, Ionics (Kiel) 23 (2017) 3377–3388.

[47] S. Monisha, T. Mathavan, S. Selvasekarapandian, A. Milton Franklin Benial, G. Aristatil, N. Mani, M. Premalatha, D. Vinoth pandi, Carbohydr Polym 157 (2017) 38–47.

[48] S. Choudhary, R.J. Sengwa, Current Applied Physics 18 (2018) 1041–1058.

[49] R. Chitra, M.V. Krishna, S. Selvasekarapandian, Polymer Bulletin (2021).

[50] M. Muthukrishnan, C. Shanthi, S. Selvasekarapandian, R. Manjuladevi, P. Perumal, P. Chrishtopher Selvin, Ionics (Kiel) 25 (2019) 203–214.

[51] H.S. Kim, T.S. Arthur, G.D. Allred, J. Zajicek, J.G. Newman, A.E. Rodnyansky, A.G. Oliver, W.C. Boggess, J. Muldoon, Nat Commun 2 (2011).

[52] L.C. Rodrigues, P.C. Barbosa, M.M. Silva, M.J. Smith, Electrochim Acta 53 (2007) 1427–1431.

[53] P.-H. Huh, M.-G. Choi, N.J. Jo, J.-K. Lee, J.-O. Lee, W. Yang, Effect of Salt Concentration on the Glass Transition Temperature and Ionic Conductivity of Poly(Ethylene Glycol)-Polyurethane/LiClO 4 Complexes, 2004.

[54] S. Monisha, S. Selvasekarapandian, T. Mathavan, A. Milton Franklin Benial, S. Manoharan, S. Karthikeyan, Journal of Materials Science: Materials in Electronics 27 (2016) 9314–9324.

[55] N.M.J. Rasali, Y. Nagao, A.S. Samsudin, Ionics (Kiel) 25 (2019) 641–654.

[56] M.F.Z. Kadir, M.H. Hamsan, Ionics (Kiel) 24 (2018) 2379–2398.

[57] A.F. Fuzlin, Y. Nagao, I.I. Misnon, A.S. Samsudin, Ionics (Kiel) 26 (2020) 1923–1938.

[58] S. Sikkanthar, S. Karthikeyan, S. Selvasekarapandian, D.V. Pandi, S. Nithya, C. Sanjeeviraja, Journal of Solid State Electrochemistry 19 (2015) 987–999.

[59] V. Moniha, M. Alagar, S. Selvasekarapandian, B. Sundaresan, R. Hemalatha, G. Boopathi, Journal of Solid State Electrochemistry 22 (2018) 3209–3223.

[60] M. Mokhtar, E.H. Majlan, A. Ahmad, S.M. Tasirin, W.R.W. Daud, J Electrochem Soc 165 (2018) A2483–A2492.

[61] M.H. Hamsan, S.B. Aziz, M.M. Nofal, M.A. Brza, R.T. Abdulwahid, J.M. Hadi, W.O. Karim, M.F.Z. Kadir, Journal of Materials Research and Technology 9 (2020) 10635–10646.

[62] N.H. Zainol, M.Z. Mohd. Halizan, W.G. Chong, Z. Osman, in: Adv Mat Res, Trans Tech Publications Ltd, 2014, 348–351.

[63] S. Rudhziah, A. Ahmad, I. Ahmad, N.S. Mohamed, Electrochim Acta 175 (2015) 162–168.

[64] M.V.L. Chandra, S. Karthikeyan, S. Selvasekarapandian, M. Premalatha, S. Monisha, Journal of Polymer Engineering 37 (2017) 617–631.

[65] S.B. Aziz, E.M.A. Dannoun, M.H. Hamsan, R.T. Abdulwahid, K. Mishra, M.M. Nofal, M.F.Z. Kadir, Membranes (Basel) 11 (2021).

[66] S.B. Aziz, M.H. Hamsan, M.M. Nofal, S. San, R.T. Abdulwahid, S.R. Saeed, M.A. Brza, M.F.Z. Kadir, S.J. Mohammed, S. Al-Zangana, Polymers (Basel) 12 (2020) 1–24.

[67] R. Narducci, Membranes 11 (2021) 159.

[68] J.B. Wagner, C. Wagner, J Chem Phys 26 (1957) 1597–1601.

[69] M.S. Mustafa, H.O. Ghareeb, S.B. Aziz, M.A. Brza, S. Al-zangana, J.M. Hadi, M.F.Z. Kadir, Membranes (Basel) 10 (2020) 1–16.

[70] M.S.A. Rani, N.S. Isa, M.H. Sainorudin, N.A. Abdullah, M. Mohammad, N. Asim, H. Razali, M.A. Ibrahim, Int J Electrochem Sci 16 (2021) 1–10.

[71] J.G. Kim, B. Son, S. Mukherjee, N. Schuppert, A. Bates, O. Kwon, M.J. Choi, H.Y. Chung, S. Park, J Power Sources 282 (2015) 299–322.

[72] P. Perumal, P. Christopher Selvin, S. Selvasekarapandian, Ionics (Kiel) 24 (2018) 3259–3270.

[73] J.B. Wagner, C. Wagner, J Chem Phys 26 (1957) 1597–1601.

[74] M.N. Hafiza, M.I.N. Isa, J Memb Sci 597 (2020).

[75] S.B. Aziz, M.A. Brza, K. Mishra, M.H. Hamsan, W.O. Karim, R.M. Abdullah, M.F.Z. Kadir, R.T. Abdulwahid, Journal of Materials Research and Technology 9 (2020) 1137–1150.

[76] S.B. Aziz, M.A. Brza, E.M.A. Dannoun, M.H. Hamsan, J.M. Hadi, M.F.Z. Kadir, R.T. Abdulwahid, Molecules 25 (2020).

[77] B.A. Boukamp, A nonlinear least squares fit procedure for analysis of immittance data of electrochemical systems, Solid State Ionics 20 (1986) 31-44.

[78] B.A. Boukamp, A package for impedance/admittance data analysis. Solid State Ionics (1986) 136-140.

[79] A. Swaminathan, R. Ravi, M. Sasikumar, M. Dasaiah, G. Hirankumar, S. Ayyasamy, Ionics (Kiel) 26 (2020) 4113–4128.

[80] R. Chitra, P. Sathya, S. Selvasekarapandian, S. Monisha, V. Moniha, S. Meyvel, Ionics (Kiel) 25 (2019) 2147–2157.

[81] V. Selvanathan, M.H. Ruslan, M. Aminuzzaman, G. Muhammad, N. Amin, K. Sopian, M. Akhtaruzzaman, Polymers (Basel) 12 (2020).

[82] M.J. Reddy, P.P. Chu, Journal of Power Sources 109 (2002) 340-346.

[83] A.S.A. Khiar, A.K. Arof, Ionics (Kiel) 16 (2010) 123–129.

[84] K.M.G. Francis, S. Subramanian, K. Shunmugavel, V. Naranappa, S.S.M. Pandian, S.C. Nadar, Polymer - Plastics Technology and Engineering 55 (2016) 25–35.

[85] R. Alves, F. Sentanin, R.C. Sabadini, M. Fernandes, V. de Zea Bermudez, A. Pawlicka, M.M. Silva, Electrochim Acta 267 (2018) 51–62.

[86] M.S.A. Rani, A. Ahmad, N.S. Mohamed, Polymer Bulletin 75 (2018) 5061–5074.

[87] M.A. Saadiah, D. Zhang, Y. Nagao, S.K. Muzakir, A.S. Samsudin, J Non Cryst Solids 511 (2019) 201–211.

[88] A.F. Fuzlin, N.M.J. Rasali, A.S. Samsudin, in: IOP Conf Ser Mater Sci Eng, Institute of Physics Publishing, 2018.